Article

Development of Mechanically Strong Ambient Pressure Dried Silica Aerogels with Optimized Properties

Hajar Maleki, Luisa Durães, and António Alberto Portugal

Just Accepted

Development of Mechanically Strong Ambient Pressure Dried Silica Aerogels with Optimized Properties

Hajar Maleki [1],*, Luisa Durães [1], António Portugal [1]

[1] *CIEPQPF, Department of Chemical Engineering, Faculty of Sciences and Technology, University of Coimbra, Rua Sílvio Lima, 3030-790 Coimbra, Portugal.*

[*]Corresponding Author

E-mail: hajar@eq.uc.pt

Tel: (+351) 910 156989

Fax: (+351) 239 798703

ABSTRACT

Ambient pressure dried (APD) silica aerogel-like monoliths with different underlying silica structures have been developed through a simple wet chemical approach. The improvement of the mechanical properties was accomplished by crosslinking the silica surface with tri-acrylate crosslinker. A solvent exchange carried out by soaking the gels in a low surface tension solvent allowed to avoid the non-safe and costly supercritical drying process. In this context, two different sets of aerogel-like monoliths have been produced and their main properties, namely bulk density, mechanical strength and thermal conductivity, were studied and modeled using the statistical Central Composite Design (CCD) approach. The empirical models derived for each property of the aerogel-like monoliths lead to further evaluation of the desirability function and optimization of silica aerogel-like properties. The key properties of the optimized APD monoliths were compared with the supercritical dried aerogels with the same synthesis conditions. Finally, the suitability of optimized silica aerogel-like and aerogel monoliths for intended space applications were further investigated by conducting several standard tests. The improved properties of the obtained APD aerogel-like monoliths render them attractive for high-technology applications, and, due to the low energy consumption of the synthesis process, they are competitive with their supercritically dried (SCD) counterparts, by presenting a best value-for-money compromise.

1. Introduction

Silica aerogels have been extensively studied due to their unique properties such as high extent of porosity (> 95%), low density (3-350 mg cm^{-3}) and very low thermal conductivity (0.004-0.03 W m^{-1} K^{-1}) [1]. Such extraordinary material properties made them suitable for the manufacturing of transparent and super insulating double windows [2, 3, 4], as well as for a number of promising aerospace and aeronautical applications [5]. The expanded industrial and commercial use of silica aerogels has been difficult to implement because of their poor mechanical properties and fragility. Moreover, the need for drying wet gels by supercritical drying (SCD) during manufacturing makes the preparation process more costly and non-safe, which limits the broadening of the aerogels applications.

The ambient pressure drying is safer and less expensive than the supercritical drying process, and has been more actively investigated in recent years [6, 7, 8, 9, 10]. Evaporation of the liquid in the pores causes serious shrinkage and cracking due to the high capillary pressure at the menisci of the solid-liquid-vapor interfaces inside the gel structure during drying. This is particularly severe when the solvent wets the solid, *i.e.* when the contact angle of the menisci is lower than 90°.

The most common approach to overcome the capillary tension is the surface modification of silica, to produce hydrophobic surfaces by reacting the silica surface hydroxyl groups with hydrophobic reagents, such as [(CH$_3$)$_3$-Si-OR] [11, 12], or hexamethyldisilazane [13, 14, 15, 16, 17, 18]. A different approach involves strengthening the gel to stand the capillary stresses. This can be achieved by replacing some of siloxane (Si-O-Si) bonds with flexible and non-hydrolysable organic bonds (Si-R), through the use of organosilanes as co-precursors to produce the aerogel network [7, 15, 19, 20, 21]. In this context, crosslinking of silica aerogels with appropriate organic polymers to prepare hybrid materials [6, 7, 8, 22, 23] was reported as an elegant and straightforward method. The organic groups on the silica surface allow the aerogel to spring

back during drying and partially recover its initial wet gel size without resulting in any cracks within the monolith structure [15, 16, 17]. Other worth mentioning approaches to overcome the induced capillary pressures involves the use of low surface tension hydrocarbon solvents [6, 9, 24], or the introduction of additives to control the drying process [25, 26]. Evaporation of a low surface tension solvent from the silica network reduces the capillary pressure when compared to the evaporation of an alcohol [27].

Enhancing silica network connectivity and/or introducing some flexible organic moieties would be a solution to overcome the capillary pressure. Recent articles list several mechanical reinforcing strategies of silica aerogels [22, 23, 28]. The polymer reinforced silica aerogels have good mechanical properties, but still are not strong enough to withstand capillary pressure when dried under ambient pressure drying condition, especially when the wet gels are dried from an alcoholic solvent. Therefore, in order to take advantages of the ambient pressure drying method to produce crack free aerogel-like monoliths with minimum dimensional shrinkage, we conducted polymer reinforcement approaches along with drying of wet gels from a low surface tension solvent.

Recently, we have studied the effect of different underlying silica structures on the physicochemical properties of tri-acrylate crosslinked supercritical CO_2 (scCO_2) dried silica aerogels [29]. The underlying silica structure was changed by altering the alkyl/aryl linker or bridge between secondary silica nanoparticles, according to the proposed molecular structures shown in Figure 1 [29]. The alkyl and aryl bridges between the secondary silica particles have been introduced by 1,6-Bis(trimethoxysilyl)hexane (BTMSH) and 1,4-Bis(triethoxysilyl)-benzene (BTESB) bis-silane precursors prior to the crosslinking reaction.
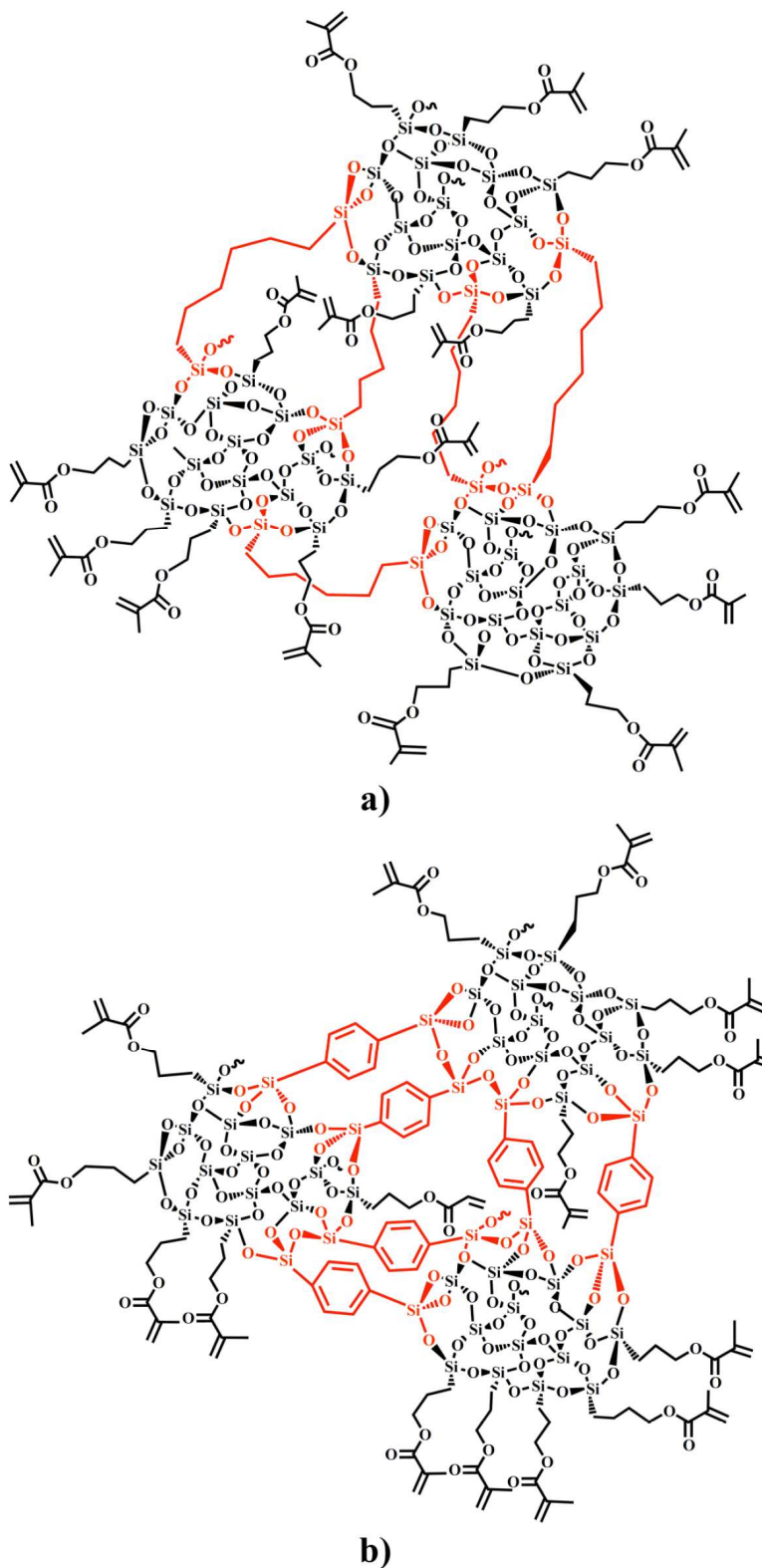
a)

b)

Figure 1. Proposed molecular structures of silica gels having a) BTMSH and b) BTESB in the underlying structure.

In the aforementioned study, we were able to show fundamental properties differences between aerogels having alkyl/aryl linking groups within the silica structure, along with a good improvement in the mechanical strength and thermal insulation performance. The aerogels made by 10 mol% of silicon derived from BTESB, which have rigid aryl spacers, show less structural collapsing during SCD. Additionally, a drastic improvement in terms of extent of porosity/pore volume and surface area and an improvement in the thermal insulation performance for such aerogels have been achieved.

Motivated by the changing of the silica aerogels properties by altering the underlying silica structure, we have also investigated safe and cost efficient synthesis of ambient pressure dried tri-acrylate reinforced silica aerogels. In order to be able to predict and control the density, mechanical strength and thermal conductivity of ambient pressure dried silica aerogels containing different underlying silica structures, optimization studies using central composite rotatable design (CCRD) of response surface methodology (RSM) were conducted.

Therefore, the aim of this study was to investigate the density, mechanical strength and thermal conductivity of ambient pressure dried tri-acrylate crosslinked aerogels and determine the effect of the type of silica precursors as well as crosslinker concentration on these properties. For this, the linear, interaction and quadratic effects of [Si]% derived from BTMSH, and BTESB and of crosslinker concentration were considered, leading to predictive models for the optimization of the test parameters. In this way, the levels of the variables using a response surface methodology (RSM) were determined.

The optimized ambient pressure dried (APD) aerogel properties were also compared with their scCO$_2$ dried counterparts for identical preparation conditions.

Our further attempt in this study was to explore the suitability of optimized aerogel-like samples for being used in Space applications, by verifying the materials specifications. For this purpose, thermal cycling and outgassing characteristics of the optimized APD aerogels

and scCO$_2$ dried aerogels were evaluated under the framework of several pre-defined standard tests.

2. Experimental

2.1 Materials

Tetramethylorthosilicate ($\geq$99%; TMOS), 3-(trimethoxysilyl)propyl methacrylate (98%; TMSPM), ammonium hydroxide (NH$_4$OH; 28-30% v/v solution), methanol (MeOH; 99.8%), hexane ($\geq$99%), ethanol (EtOH; $\geq$99.5%), tris[2-(acryloyloxy)ethyl]isocyanurate (99%), 2,2′-azobis(2- methylpropionitrile) (98%; AIBN), 1,4 - Bis(triethoxysilyl)-benzene (96%; BTESB) and acetone were purchased from Aldrich. 1,6 - Bis(trimethoxysilyl) hexane (98%; BTMSH) was purchased from Cymit. All reagents were used without further purification.

2.2 Methods
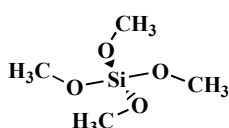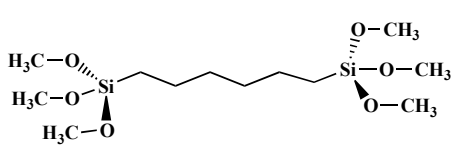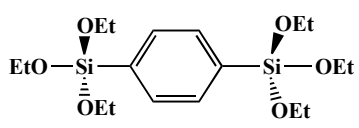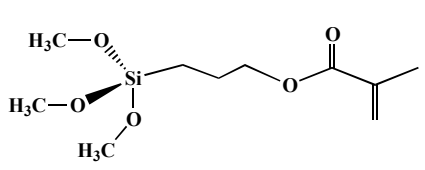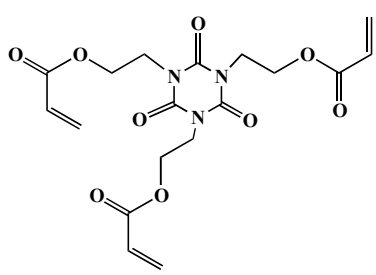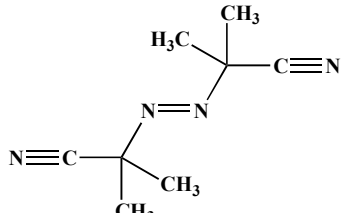
2.2.1 General

Variables used in this study include the bis-silane type (BTMSH, BTESB), the mole fraction of the total silicon derived from BTMSH and BTESB (note that these precursors contribute with two silicon atoms in every molecule, and the rest of the silicon is derived from TMOS and TMSPM). The amount of silicon derived from BTMSH varied from 0 to 40 mol%; in the aerogel derived from BTESB, the amount of silicon from BTESB had values of 5 to 10 mol% of the total silicon. The amount of crosslinker (tri-acrylate) was given as mole fraction to TMSPM (R) and varied from 0.5 to 2. The water/total silicon mole ratio (r) was kept at a value of 4 for all formulations, which is higher than the stoichiometric value for

hydrolysis and condensation of TMOS ($r = 2$). Whole reagents used in this work with their

molecular structures and abbreviations are listed in Table 1.

Table 1. List of chemical structures of all used reagents along with their abbreviations.

Chemical structure	Name	Abbreviation
	Tetramethylorthosilicate	TMOS
	1,6 - Bis(trimethoxysilyl) hexane	BTMSH
	1,4 - Bis(triethoxysilyl)-benzene	BTESB
	3-(trimethoxysilyl)propyl methacrylate	TMSPM
	tris[2-(acryloyloxy)ethyl]isocyanurate	Tri-acrylate
	2,2′-azobis(2-methylpropionitrile)	AIBN

2.2.2 Preparation of polymer-reinforced ambient pressure dried (APD) silica aerogel-like monoliths

Apart from the drying step, the mechanically reinforced APD aerogels monoliths of this study followed the same synthesis procedure as their scCO$_2$ dried counterparts, which is reported elsewhere [29]. For reference, a typical procedure is outlined for a formulation with total silicon concentration of 1.3 mol/L in the sol, a BTMSH Si fraction of 40 mol% and the tri-acrylate monomer in a 1.25 ratio to TMSPM (Run B_40_R_1.25 of Table 3). A solution of 1.52 mL (10.56 mmol) of TMOS, 1.74 mL (10.56 mmol) of BTMSH, and 1.19 mL (5.2 mmol) of TMSPM was cooled to below 0°C in an ethanol mixed dried-ice bath (Solution 1). Solution 2 was prepared by adding 12.9 mL of the gelation solvent (methanol), 2.7 g of Tris[2-(acryloyloxy)ethyl] isocyanurate monomer, water ($r = 4$), 0.7 mL of NH$_4$OH solution and 0.27 g of AIBN (formulated to be 10 wt% of the organic monomer). The two solutions were mixed and poured into two propylene cylindrical molds, with 17.2 mm nominal diameter. The gels were formed within 5 min to 2 hours depending on the formulation. After 24 hours of aging, the wet gel was demolded and placed in a cylindrical reaction flask, containing enough ethanol solvent to cover the gel and the same concentration of initiator used in the gelation step. The sample was refluxed at 70°C, for 6 hours, to promote free radical polymerization of the organic monomers inside the pores of the wet gel with silica surface functionalities. After crosslinking, in order to remove the residual water and ethanol, the samples were washed three times with the gelation solvent, giving 8 hours interval between each washing step. Afterwards, methanol was slowly exchanged by hexane over a 24 hours period. Finally, the wet gels were carefully placed in the ventilated oven and dried several days in ambient pressure and temperature conditions.

The experimental procedure leading to the BTESB derived aerogel-like sample was exactly similar to the procedure described above. The only difference is in the preparation of Solution 1, in which the BTESB precursor with defined silicon mole percentages has been introduced to the solution instead of the BTMSH precursor.

2.3 Physicochemical analysis

Solid-state ^{29}Si and ^{13}C NMR spectra of the aerogels were obtained by an *Inova 500* spectrometer using a 4 mm solids probe with cross-polarization and magic angle spinning at 11 kHz. Infrared analysis was conducted with ATR-FTIR spectroscopy (*JASCO FTIR-4100*).

The bulk density (ρ_b) was determined by measuring the weight and volume of the sample. Dimensional shrinkage (%) was taken as the difference between the diameters of the aerogel monolith and of the 20 mL syringe mold (nominally 17.2 mm). He pycnometry (*Accupyc 1330, Micromeritics*) was used to measure the real (skeleton) density of the samples. Combining the information of the skeleton and bulk densities, it was possible to evaluate the porosity and pore volume of the samples through equation (1) and (2), respectively:

$$Porosity\ (\%) = \frac{\frac{1}{\rho_b} - \frac{1}{\rho_s}}{\frac{1}{\rho_b}} \times 100 \tag{1}$$

$$Pore\ volume\ (cm^3\ g^{-1}) = \frac{1}{\rho_b} - \frac{1}{\rho_s} \tag{2}$$

In addition, we used the Nitrogen gas adsorption (*Accelerated Surface Area and Porosimetry ASAP 2000, Micromeritics*) for the determination of the specific surface area. Before the analysis, the sample was outgassed at 60°C in vacuum (10^{-5} bar) during 24 h, to remove adsorbed species. In the analysis, volumes of the adsorbed nitrogen at five different

relative pressures (0.05 to 0.2) were taken at 77 K, to obtain the specific surface area by the

BET theory. The average pore diameter of samples has been calculated from equation (3):

$$Average\ pore\ diameter\ (nm) = \frac{4\ (pore\ volume)}{S_{BET}} \tag{3}$$

Scanning electron microscopy (SEM) (*JMS-5310, JOEL*) was used to observe the materials

microstructure. Due to the low electrical conductivity of the highly porous silica-based

samples, an Au film was deposited on their surfaces, using the Physical Vapor Deposition

(PVD) technique during 20 s.

The thermal conductivity of the reinforced aerogels was measured using a transient method

(*Thermal constants analyzer TPS 2500 S, Hot Disk*). The sensor is clamped between two

identical disc shaped pieces of the sample, which have a diameter of 1 cm and thickness of

0.5 cm (conveniently cut from the cylindrical aerogel samples). This analysis was carried out

at 20ºC and the equipment presents a reproducibility and accuracy over 1% and 5%,

respectively.

For the mechanical test, samples were cut to meet a length:diameter ratio of 2:1, and were

polished to make sure that top and bottom sides were smooth and parallel. The compression

test was conducted following the *ASTM standard D695-02a*. All tests were done at nominal

room conditions with a stroke speed of 1.3 mm/min.

2.4 Vacuum outgassing and thermal cycling screening tests

The thermal characteristics of developed aerogels have been evaluated by conducting two

standard screening tests of vacuum outgassing (normative reference: *ECSS Q ST 70 02C*,

European Space Agency for the members of ECSS, 2008) and thermal cycling (normative

reference: *ECSS Q ST 70 04*, European Space Agency for the members of ECSS, 2008).

The two standard tests of vacuum outgassing and thermal cycling have been conducted in a

vacuum drying oven (*Binder;* temperature range: 15°C (59°F) - 200°C (392°F); heating rate:

3°C min^{-1}; pressure interval: 1 mbar - 1 atm).

Before conducting the standard tests, for each selected optimized aerogel and aerogel-like

monoliths under study, three specimens (replicas) with minimum weight of 0.1 g were

prepared by proper cutting from initial monoliths. For the outgassing test, after recording the

initial weight of each sample (~0.3 g), the Total Mass Loss (TML) of the material outgassed

during 24 hours, at constant temperature of 125°C and minimum pressure of 1 mbar was

evaluated. The Water Vapor Regained (WVR), which is defined as the mass of water vapor

regained by the sample after a reconditioning step, is measured from the increase in the

sample mass, after the test for TML, when exposed 2 hours to controlled conditions (relative

humidity of 65% at room temperature of 22°C). The total mass of the specimen without

adsorbed water, *i.e.* the Recovered Mass Loss (RML), is evaluated by the previous two

quantities, according to the following expression:

RML = TML – WVR   (4)

The outgassing requirement is RML < 1% in order to consider the material acceptable for

use in Space applications.

After evaluating the values of TML, WVR and RML, the samples chemical properties were

evaluated again by taking ATR FT-IR spectra.

For the thermal cycling test, for each selected sample, three replicas were prepared and

precisely weighted, and then, samples were exposed to three successive thermal cycles from -

78°C to 125°C. To do this, firstly the samples were immersed in liquid nitrogen (-78°C) for

about 1 min and, then, they were allowed to rest at ambient temperature for 30 min. After, the

samples temperature was raised to 125°C in an oven, for 30 min, under vacuum. This

procedure was repeated for each sample after allowing the sample to rest in ambient

conditions for 2 hours. After each cycle, the information related to the sample outgassing and

macroscopic changes in the samples was recorded.

2.5 Central Composite Rotatable Design (CCRD)

Experimental design and analysis was conducted using *Design Expert 7.1.3* available from

State-Ease, Inc. (Minneapolis).

Two 2-factor-5-level central composite rotatable designs (CCRD) with two replicas at the

center were used to develop predictive models for some physical and mechanical property

parameters of BTMSH and BTESB derived aerogels. It was deemed reasonable to set two

CCRD for each type of APD-aerogel-like samples (with BTMSH or BTESB) to evaluate

measured properties of crosslinked aerogels as a function of processing parameters. The two

factors' levels in terms of coded and uncoded (actual) values are shown in Table 2 and Figure

2 for BTMSH and BTESB derived aerogels.

Here in, the important variables under study as well as their levels have been previously

defined by factor screening. Therefore, for each ambient pressure dried aerogel, two

preparation conditions have been systematically varied: silicon concentration derived from

BTMSH or BTESB (X_1) and values of R, which are defined as a molar ratio of tri-acrylate to

TMSPM (X_2). The variation of these two variables has previously demonstrated to have a

strong effect on both mesoporous underlying structure and the extent of crosslinking [29].

This design includes a standard of $2k$ factorial points (coded as ±1 notation), $2k$ points fixed

axially at a distance *a* from the center (±*a*), and N_0 replicate tests at the center (0) – Figure 2. *k*

is the number of operating variables. Center points, which are located in the midpoint of each

factor range, give information about the existence of curvature. The total number of design

points in CCRD (*N*) can be calculated from:

$N=2k+2k+N_0$ (5)

Table 2. Coded and actual levels of variables considered for design for APD BTMSH and

BTESB derived aerogel-like monoliths.

Feed Factors	Coded X_i	BTMSH derived aerogel-like material					BTESB derived aerogel-like material				
		Variation levels					Variation levels				
		-1.41	-1	0	1	1.41	-1.41	-1	0	1	1.41
Si mol% of Bis-silane	X_1	0	6%	20%	34%	40%	5%	6%	7.5%	9%	10%
R	X_2	0.5	0.7	1.25	1.8	2	0.5	0.7	1.25	1.8	2
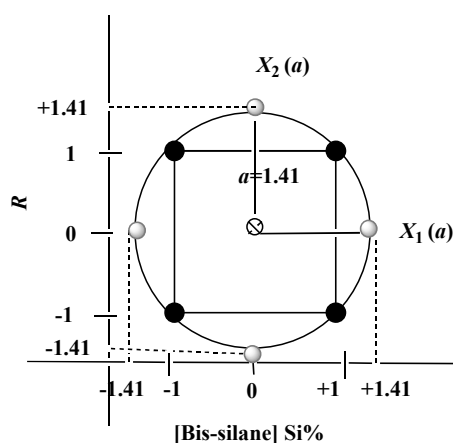
● **2² factorial points** ○ **Axial points** ⊗ **Center points**

Figure 2. Central composite rotatable design (CCRD) for two experimental factors, X_1 and X_2

variables, respectively Si mol% derived from BTMSH and BTESB, and R ratio.

The estimation of the pure quadratic properties of the model can be carried out by using the

axial points. All these points were calculated as function of the range of interest for each

factor [30].

Rotatability was selected since its properties of the design are desirable. The design is

rotatable if the variance of response is constant for all variables at a given distance from the

design center [31]. The CCRD is rotatable if:

$$\alpha = \sqrt[4]{2^k} \tag{6}$$

The X_1 and X_2 variables were orthogonalized (transformed to -1 to 1 range) prior to the modeling, in order to minimize correlation between terms. The results were statistically evaluated by the analysis of variance (ANOVA) at the significance level of $p=0.1$ or 90% confidence. The software calculates F-test for significance of the model as well as the significance of each term. Apart from calculating p-values, the adequacy of the model was also evaluated by the coefficient of determination (R^2). The R-squared value of the final model indicates the amount of variation present around the mean that is explained by the model. The closer R-squared is to 1, the less variation exists around the model. The standard deviation of the model is also given. The standard deviation reported is the square root of the residual mean square, and is taken as an estimate of the standard deviation of the experiment.

Multiple regression analysis was used and the second order polynomial equations as function of X_i were fitted for each variable assessed at each experimental point. The second-order polynomial equation was:

$$y = (\beta_0 + \varepsilon) + \sum_{i=1}^{2} \beta_i X_i + \sum_{i=1}^{2} \beta_{ii} X_i^2 + \sum_{\substack{i=1 \\ i<j}} \sum_{j=i+1} \beta_{ij} X_i X_j \tag{7}$$

Where y is the estimated (predicted) response; ε is the random error, β_0 is average value of the response at the center points of design; β_1, β_2, $\beta_{1,2}$, β_{11} and β_{22} are linear interactions and quadratic terms, respectively, which were empirically derived from the experimental data.
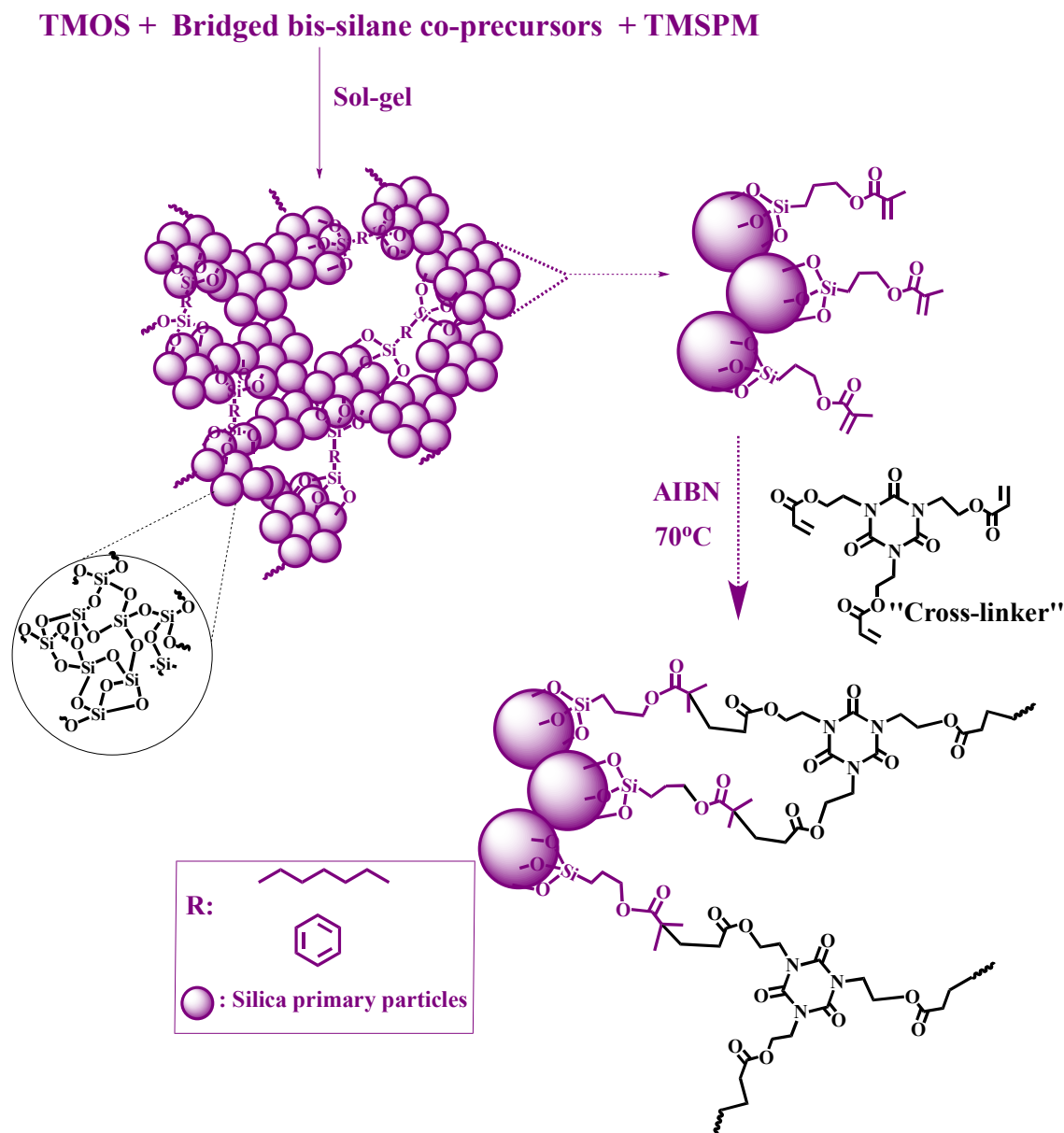
3. Results and discussion

As previously described [29], the multifunctional acrylate crosslinked silica aerogels were prepared firstly by reacting a mixture of tetramethylorthosilicate (TMOS), bis-silane precursors and 3-(trimethoxysilyl) propyl methacrylate (TMSPM), with base catalysis, to form a silica backbone, following by polymerization on the silica surface as shown in Figure

3. TMSPM was incorporated as a site for tri-acrylate crosslinking in these gels. This approach of silica surface functionalization was also adopted in the very recent study made by Bertino *et al.* [32] that opted for such a synthesis strategy for their water/ethanol azeotrope SCD crosslinked aerogels, further confirming the feasibility of such strategy.

In this study, because the tri-acrylate crosslinker is soluble in methanol (gelation solvent) and due to the non-ionic free radical polymerization (compared to the ionic nature for the sol-gel process), we added the crosslinker to the gelation solvent in the initial step of preparation of the sol. Then, free radical polymerization occurs after the sol-gel process by applying post-gelation thermal treatment to the wet silica gels. The idea of one pot development of strong aerogels has been firstly established by Mulik *et al.* [33] and led to a significant time reduction in the synthesis and processing of aerogels. In their study, the polymerization was confined only to the silica surface by promoting so-called surface initiated free radical polymerization (SIP) technique from the silica surface. Although the aerogels were stronger when compared to the aerogels that were prepared in our group [29, 34], the material was denser and the proposed preparation methodology was tedious which turns their approach less interesting for mass production.

With all crosslinking methodologies, being able to probe the exact location of the polymer or the scale of the polymerization reaction in the silica matrix is important, and recently it has been a challenging matter [35, 36]. No single characterization was sufficient to address this complex issue, hence, in this study, the nanostructure is probed chemically at the molecular level by FT-IR, ^{13}C, and ^{29}Si NMR and at nanoscopic level by SEM and TEM [29].

TMOS + Bridged bis-silane co-precursors + TMSPM

Sol-gel

AIBN
70°C

"Cross-linker"

R:

: Silica primary particles

Figure 3. Proposed crosslinking scheme with TMSPM and tri-acrylate.

3. 1 Chemical characterization

The chemical structures of the aerogels as well as the extent of crosslinking with various underlying silica structures were characterized by studying the solid-state ^{13}C NMR [29], solid-state ^{29}Si NMR and ATR FT-IR spectra.
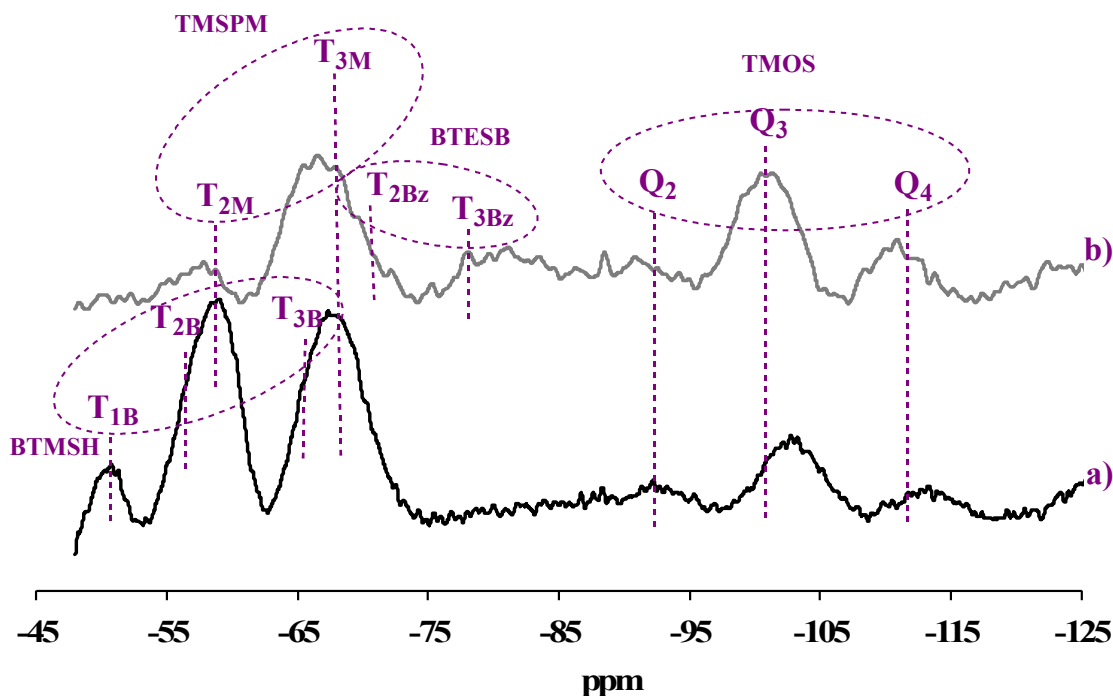
Figure 4. Solid-state ^{29}Si NMR spectra of aerogel-like samples: a) B_40_R_1.25, which is assigned for the sample containing TMOS 40 mol% + BTMSH 40 mol% + TMSPM 20 mol%, b) Bz_10_R_1.25 which is assigned for the sample with TMOS 70 mol% + BTESB 10 mol% + TMSPM 20 mol%.

The solid ^{29}Si NMR spectra for the aerogel-like samples in which 40 mol% of total silicon was derived from BTMSH (Figure 4a), and, 10 mol% of total silicon derived from BTESB (Figure 4b), with the rest of silicon derived from TMOS and TMSPM precursors, are shown to study the reactivity of each silica precursor. The characteristic peaks that belong to TMOS are assigned as Q_n, being ''n'' indicative of the degree of condensation of silica or extent of siloxane bond (''Si-O-Si'') formation. The T_{nM}, T_{nB} and T_{nBz} are assigned to the characteristic peaks for TMSPM, BTMSH and BTESB precursors, respectively, with ''n'' being the number of siloxane bonds in each precursor.

The ^{29}Si spectrum for both aerogel-like samples consists of three peaks Q_4, Q_3 and Q_2, being the largest population from Q_3 sites at -101 ppm, which is indicating that a large

number of Si-OH sites in TMOS have undergone a condensation reaction. Also, the peak at

T_{2M} (-61 ppm) integrates about half of the area of peak T_{3M} (-69 ppm), indicating that 2/3 of

TMSPM silicon atoms had completely reacted. Referring to Figure 4a and by subtracting T_{nM}

peaks (by considering the equivalent peak areas in Figure 4b), the area of the T_{2B} peak at -58

ppm is to some extent larger than T_{3B} at -67 ppm. Therefore, it can be concluded that more

than half of BTMSH silicon atoms are not fully reacted. In the spectrum b, the T_{2Bz} peak at -

71 ppm is strongly overlapped with the T_{3M} and has slightly larger peak area than T_{3Bz}, at -78

ppm, which indicates an incomplete condensation of BTESB during sol-gel reaction.

ATR FT-IR spectra of the different monoliths show that at $R = 2$, almost all silica surface

carbon double bonds, at 1628 cm^{-1}, are consumed during the crosslinking reaction – Figure

SI_1a-c. As expected, a peak due to the stretching vibration of C=O bonds of tri-acrylate at

1690 cm^{-1} has appeared (*vd.* Figure SI_1b, d). This is evidenced by the increasing area under

the characteristic peak of tri-acrylate on the solid-state ^{13}C NMR spectrum and, in the thermo

gravimetric analysis, by a drastic increase in the weight loss due to the crosslinker in the

aerogel composites [29]. The average number of monomer units (N_t), along with the mass

percentage of the monomer contribution on the composites, for representative samples of this

study containing different underlying silica at $R = 2$, were quantified and summarized in

Table 3. In the crosslinked aerogels without bis-silane precursors in the underlying silica, the

extent of crosslinking is relatively higher than for those containing BTMSH and BTESB bis-

silanes. The relative poor crosslinking reaction in the aerogel-like monoliths containing

BTMSH may be due to the less accessibility of the silica surface methacrylate to the

crosslinker, being sterically blocked by hexyl links from BTMSH [37].

To locate the polymerization reaction scale in the silica backbone, besides the chemical

characterizations, a wide array of characterization techniques is also required. Mohite *et al.* [36]

have recently addressed this issue using ring opening polymerization of norbornene on the

silica surface. In analogy with this study and having the chemical make up of the silica

skeleton in the molecular scale along with visualizing the microscopy results [29], it can be

assumed that silica backbone consist of secondary particles having core-shell primary silica-

polymer particles in which empty spaces between these primary particles filled either by air or

loosed polymer of different density.

Table 3. Monomer contribution in the different aerogel-like composites.

	Crosslinked_ BTMSH 40 mol%, $R=2$	Crosslinked_ BTESB 10 mol%, $R=2$	Crosslinked_ without bis-silane, $R=2$
Average number of monomer units (N_t)	1.7	2.5	3.2
Crosslinker (wt%) in the aerogel composites	23%	32%	41%

Hydrophobic behavior of some selected best samples was evaluated by studying their water

contact angle values. As shown in Figure 5, contact angles measured for representative

samples in this study ranged from 100 to 151°. The high contact angle (151±15°) for BTMSH

derived gels indicates that the hexyl groups from BTMSH are present in the silica surface and

contributed to the hydrophobic nature of the crosslinked aerogels. The surface of such a

aerogel sample is exhibiting petal effect [38], sticking the water to the surface even with tilting

upside down the sample, which is a characteristic of surfaces with superhydrophobic nature

(nonwettable). Additionally, the contact angle measured for this sample is higher than for its

scCO$_2$ counterpart ($\theta = 102\pm2°$), suggesting the importance of the drying condition on the

hydrophobic properties of this material. A very recent study by Leventis et al. [39] indicated that

hydrophobicity is well correlated with morphostructure of aerogel materials. Herein,

macroscopic dimensional shrinkage upon APD may induce different textural properties on the

monoliths and, therefore, result in alteration of both morphology and surface energy which in

turn may render different hydrophobicity results compared to the aerogels counterparts [40]. The

contact angle measured here is comparable with those reported in the recent state of the art

aerogels (*e.g.*, styrene reinforced aerogels [37, 41], texture induced polyurea (PUA) aerogels [39]).

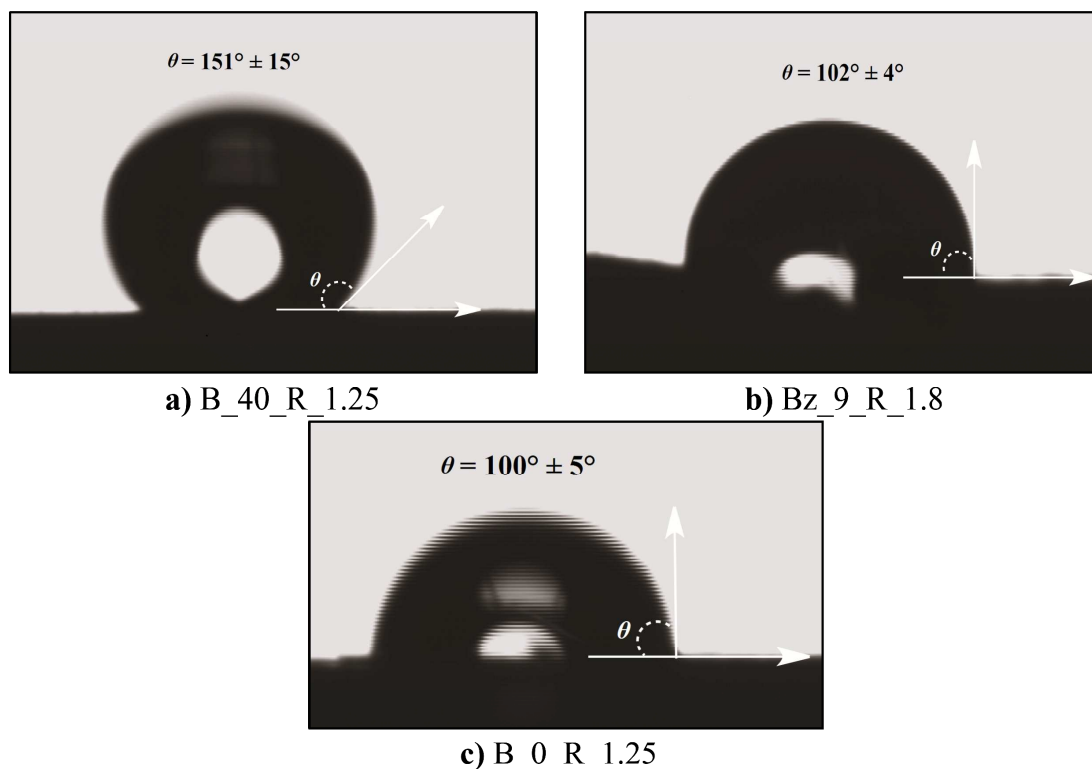a) B_40_R_1.25   b) Bz_9_R_1.8

c) B_0_R_1.25

Figure 5. Water contact angle measurements for the crosslinked aerogel-likes with and

without BTMSH and BTESB precursors.

3.2 Modeling the responses for BTMSH and BTESB derived aerogel-like materials

Properties of different polymer-reinforced silica aerogels have been previously studied and

modeled by full factorial design [42, 43, 44, 45] and d–optimal design [37, 46, 47] strategies in which,

with later design, the synthesis parameters have been optimized by minimum experimental

trials. Moreover, it is a computer-generated method. The experiments that were carried out

here are according to a Central Composite Rotatable Design (CCRD), which is the most

popular and versatile optimal design and allows the calculation of linear and quadratic effects

and interactions of factors with the best possible precision at a minimum number of

experiments. In this work, for each aerogel-like samples, 10 experimental runs were prepared.

The bis-silane silicon mol% in terms of BTMSH derived aerogel-like materials was varied

from 0 to 40% of total silicon, while for BTESB derived aerogels, it was varied from 5 to

10% of total silicon. The R values ranged from 0.5 to 2. The samples were characterized in

terms of bulk density, thermal conductivity and maximum strength at break and the results are

summarized in Table 4.

By using the multiple regression analysis, the second order polynomial equations as

function of X_i were fitted for each variable assessed at each experimental point.

Table 4. Coded operating variables with measured properties of BTMSH and BTESB derived

aerogel-like monoliths.

Run no.	Coded level of variables		Experimental responses of BTMSH derived aerogel–like monoliths		
	$X_1{}^a$	$X_2{}^b$	Density (g cm^{-3})	Thermal conductivity (W/m^{-1} K^{-1})	Max. stress at break (MPa)
B^c_20_R_1.25	0	0	0.50	0.079	2.80
B_20_R_1.25	0	0	0.54	0.081	3.20
B_6_R_0.7	-1	-1	0.48	0.071	0.31
B_34_R_0.7	1	-1	0.46	0.057	2.01
B_6_R_1.8	-1	1	0.66	0.101	1.12
B_34_R_1.8	1	1	0.34	0.065	0.59
B_0_R_1.25	-1.14	0	0.78	0.130	1.13
B_40_R_1.25	1.14	0	0.25	0.055	0.79
B_20_R_0.5	0	-1.14	0.52	0.088	1.03
B_20_R_2	0	1.14	0.56	0.073	4.00
Run no.	Coded level of variables		Experimental responses of BTESB derived aerogel-likes monoliths		
	$X_1{}^a$	$X_2{}^b$	Density (g cm^{-3})	Thermal conductivity (W/m^{-1} K^{-1})	Max. stress at break (MPa)
Bz^d_7.5_R_1.25	0	0	0.65	0.096	3.61

Bz_7.5_R_1.25	0	0	0.70	0.127	3.60
Bz_6_R_0.7	-1	-1	0.71	0.133	0.30
Bz_9_R_0.7	1	-1	0.64	0.105	0.20
Bz_6_R_1.8	-1	1	0.73	0.103	4.20
Bz_9_R_1.8	1	1	0.58	0.075	2.70
Bz_5_R_1.25	-1.14	0	0.79	0.138	0.34
Bz_10_R_1.25	1.14	0	0.68	0.096	3.30
Bz_7.5_R_0.5	0	-1.14	0.61	0.113	0.13
Bz_7.5_R_2	0	1.14	1.05	0.079	3.80

[a]X_1: Si mol % derived from BTMSH or BTESB
[b]X_2: R = [Tri-acryl]/[TMSPM]
[c]B: BTMSH [d]Bz: BTESB

Summary statistics and significant terms in the models along with the final fitted models of each response/property for both types of aerogel-like samples are shown in Table 5.

Table 5. Significant terms and statistics summary of response surface models for BTMSH derived aerogel-like material and BTESB derived aerogel-like material.

BTMSH derived aerogels	Significant terms	R^2	Standard error (RMS)	Fitted model
Density	X_1, X_1X_2	0.89	0.061	Density = $0.41+3.12\times10^{-3}$[B]-0.01[B]R
Maximum stress at break (power transformed)	X_1X_2	0.80	2.400	(Max.stress at break)$^{-2}$ = 15.6+0.40[B]R
Thermal conductivity	X_1	0.82	0.009	Thermal Conductivity = $0.10-1.37\times10^{-3}$[B]

BTESB derived aerogels	Significant terms	R^2	Standard error (RMS)	Fitted model
Density	X_2	0.81	0.040	Density = 0.70+0.15R
Maximum stress at break (power transformed)	X_2, X_2^2	0.91	1.200	(Max.stress at break)$^{-1}$ = 21.82-16.94R+6.34R^2
Thermal conductivity	X_1, X_2, X_1^2, X_2^2	0.99	0.001	Thermal Conductivity = 0.32-0.50[Bz]-0.01R+2.70×10^{-3}[Bz]^2-6.50×10^{-3}R^2

Response surface plots were generated with the *Sigma Plot* software (*SigmaPlot 12.0*) and drawn by using the function of two factors. Note that the axes in the resulting surface response plots are sometimes rotated in order to best illustrate the particular surface. Therefore, with the derived empirical response surface models, significant effects of the variables on the measured properties were assessed.

Graphs of the response surface models for bulk density, mechanical strength and thermal conductivity are shown in Figure 6. These are plotted vs. mol% of Si derived from bis-silane and *R* ratio. As it is evident from Figure 6a and Table 5, and in agreement with previous studies, the most influential variable on the density of BTMSH derived aerogels is the percentage of BTMSH as well as the synergetic effect of the percentage of BTMSH and *R*. This is due to the insertion of additional mass of BTMSH and crosslinker on the aerogel-like samples. However, in terms of BTESB derived aerogels, due to the low incorporation of BTESB precursor, there is a less significant effect of bis-silane concentration on the measured density – Figure 6d and Table 5. The main influential factor in this case is *R*, and density increased positively by increasing the tri-acrylate crosslinker concentration. In addition, for the same preparation conditions, the bulk densities for these aerogel-like samples exceed the values for BTMSH derived counterparts. This is due to the substantial increase in the extent of crosslinking/number of repeating units incorporated per TMSPM unit as measured by solid ^{13}C NMR and TGA for BTESB derived aerogels (Table 3). The actual effect of tri-acrylate concentration on the density of these aerogels is a challenge, since these samples suffered a high level of shrinkage during the course of drying.

The BTMSH derived aerogels displayed the less structural collapsing, with an average dimensional shrinkage of 20% upon ambient pressure drying, while BTESB derived aerogels showed an average shrinkage value as high as 30%. This effect is particularly visible at low crosslinker concentrations. Therefore, the increase in density for the BTESB derived aerogels

is somehow related to the extent of dimensional shrinkage, as well. Due to the flexible nature of hexyl groups in the BTMSH derived monoliths, these samples recovered most part of their initial wet gel sizes after the ambient pressure drying process.

The graphs of the response surface models for mechanical strength for both aerogel-like samples is shown in Figure 6b, e. As indicated, the most dominant factor in the mechanical strength of BTMSH based aerogel-like sample is the synergetic effect of BTMSH percentage with crosslinker concentration (Figure 6b, Table 5). In fact, the model indicates that with an increasing molar percentage of BTMSH, the compression strength increases when crosslinker concentration is high, but the inverse occurs when the crosslinker concentration is low. In terms of BTESB derived aerogels, first and second order effects of crosslinker concentration have significant effects on the mechanical strength – Figure 6e, Table 5.
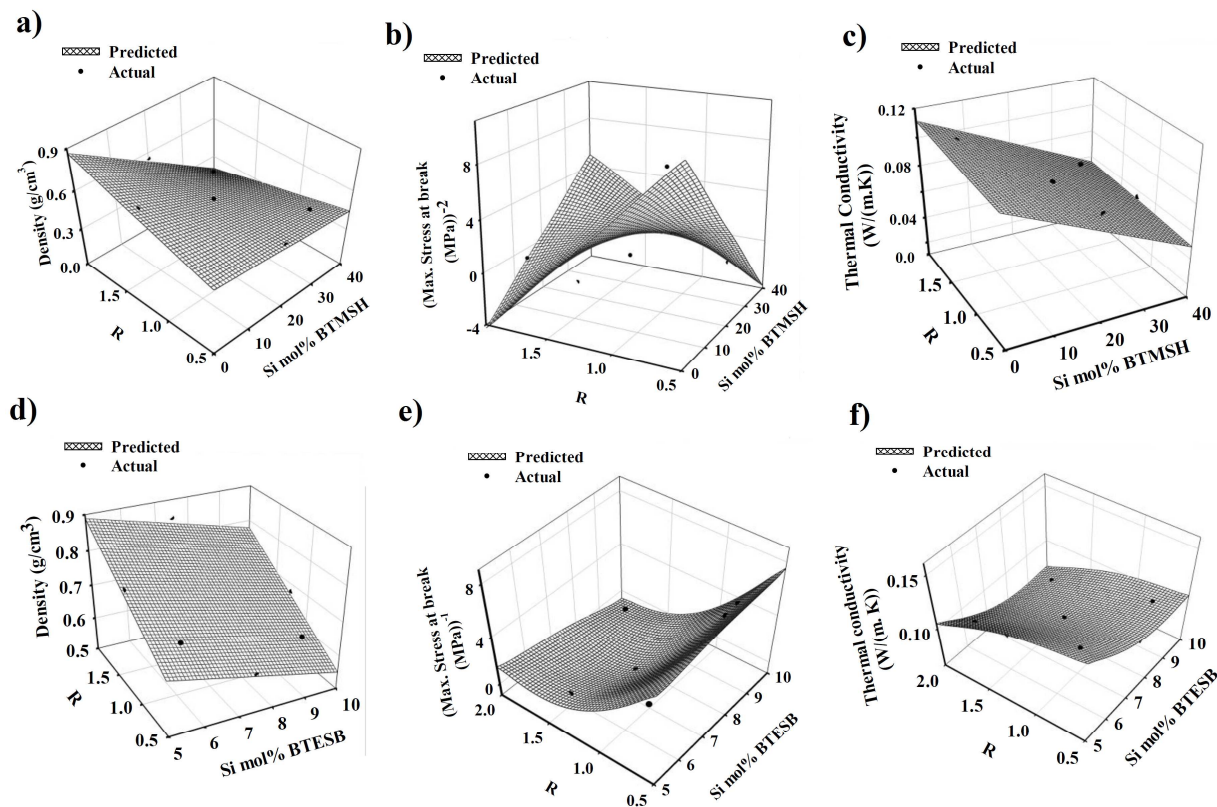
a)

b)

c)

d)

e)

f)

Figure 6. Response surface models of a) density, b) mechanical strength and c) thermal

conductivity of BTMSH derived APD-aerogel-like monoliths versus the mol% of silicon from

BTMSH and *R;* response surface models of d) density, e) mechanical strength and f) thermal

conductivity of BTESB derived APD-aerogel-like monoliths versus the mol% of silicon from

BTESB and *R*.

The BTESB derived aerogels are stiffer (Young's modulus (*E*) ~ 0.05-1.8 MPa) when

compared to the BTMSH derived aerogels (*E* ~ 0.01-0.43 MPa), due to the presence of rigid

aryl spacer in their structures - Figure SI_2a, b. Moreover, high extent of shrinkage in the

APD process intensified this property.

As expected, thermal conductivity is mostly influenced by the percentage of the BTMSH

(Figure 6c), in agreement with results from another reported work [29]. Upon increasing

BTMSH molar percentage, the silica network has undergone less structural shrinkage, which

led to large spacing between silica secondary particles, and therefore thermal insulation

performance of aerogel-like monoliths has subsequently improved. Response surface graph of

thermal conductivity for BTESB derived aerogels (Figure 6f) indicates that, both the

underlying silica structure and R have contribution to the thermal conductivity values of this

type of aerogel-like samples. The effect of BTESB concentration can be better observed

specially at R = 2, where the thermal conductivity decreases with the increasing of BTESB

derived Si mol% from 5 to 10 mol%. This is probably due to the increase in the porosity

values due to the rigid aryl spacer. Higher porosity favors low thermal conductivity, despite

the drastic increase in the density upon drying for these aerogels.

　The N_2 adsorption isotherms along with the pore volume, mean pore sizes and extent of

porosity of some selected aerogel-like samples having the same crosslinker concentration but

different underlying silica structures are shown in Figure 7 and Table SI_1, respectively. The

N_2 adsorption volumes, the pore sizes and the porosity are extremely influenced by the degree

of crosslinking as well as by the inorganic silica nanostructure. As indicated in Figure 7, in

the crosslinked aerogels, the N_2 adsorption volumes decreased due to the closing of the

network pores upon crosslinking by polymer. The reinforced BTESB aerogel-like samples,

like their $scCO_2$ dried aerogels, despite the higher extent of polymerization on their surfaces

(higher than the reinforced BTMSH aerogels), exhibited relatively high adsorption volumes

and, consequently, high specific surface areas. Such aerogels possess also relatively high

extent of porosity (Table SI_1) and, length scales of the pores (40 nm) are smaller than the

mean free path of air molecules at standard temperature and pressure ($\approx$ 80 nm). Therefore,

improvement in the thermal insulation performance of this type of monoliths is expected, due

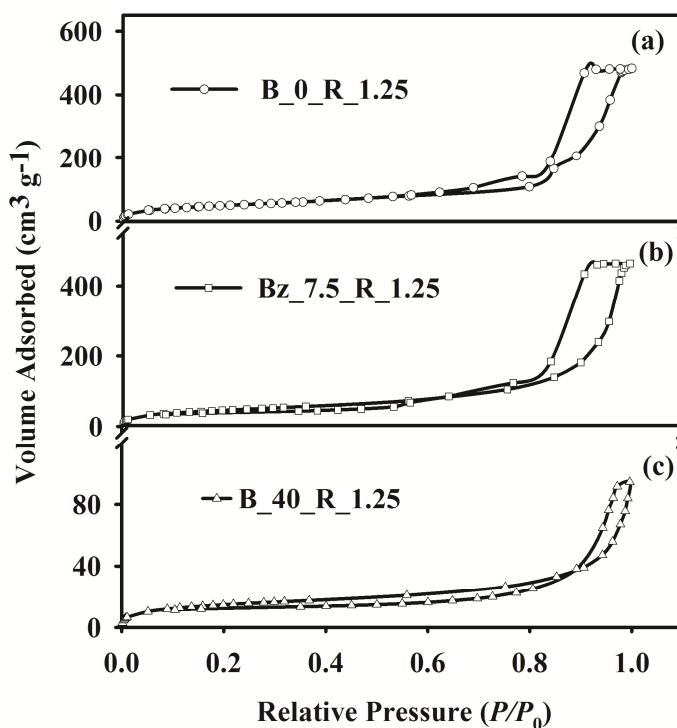to a decrease in the gaseous component of thermal conductivity.

Figure 7. Comparative N$_2$ sorption isotherms of selected crosslinked APD-aerogel-like

monoliths.

3.3 Optimization of the properties of ambient pressure dried BTMSH and BTESB

derived aerogel-like samples

Optimization is an essential tool in the development of silica aerogels for the efficient

adjustment of different important synthesis parameters to yield highly acceptable material

properties. Optimization and adjustment of the mechanical properties of silica aerogels is a

challenge due to the trade off between mechanical strength and bulk density and, therefore,

thermal conductivity [28]. So, optimization of silica aerogels properties during mechanical

reinforcement, preserving their initial important properties, must be carried out.

Here in, during the optimization of synthesis parameters of APD-aerogel-likes, several

response properties describe the quality characteristics of the obtained samples. Some of these

properties need to be maximized, while others need to be minimized. To optimize the process

with two or more output responses, it is helpful to use the concept of desirability function [48].

The desirability function is one of the most widely used methods for optimization of multiple

response processes in science and engineering [49]. Desirability varies from zero to one for

specific responses. A value of one represents the ideal case (fully desired response), while

zero indicates that one or more responses fall outside the desirable limits (completely

undesired response).

The main goal of this research was to find the best preparation conditions for the

development of APD-aerogel-like samples with material properties near to their $scCO_2$ dried

aerogel counterparts. In this context, the desirability allows to find the optimal bis-silanes

type and their percentage along with optimal crosslinker concentration.

The desirability function for both aerogel-like types was adopted for the following criteria:

maximum value for the compression strength and minimum values for density and thermal

conductivity. In terms of density and thermal conductivity, the weight of responses are set at 5

which is determining the level of importance of these two responses in order to be close as

possible to the minimum. In terms of maximum strength, the weight of response is set at 3 in

order to be close as possible to the maximum.

By applying the desirability function method, the optimum preparation conditions are

demonstrated in Figure 8a, b and Table 6 and were found to be the following: for APD-

BTMSH derived aerogels, the BTMSH Si mol% was 40 % and the R value was 1.56; for

APD-BTESB derived aerogels, the BTESB Si mol% was 9.27 % and the R value was 1.8.

From the response surface graph of desirability for BTMSH aerogel-like monoliths, the

optimum density was determined as 0.26 g cm^{-3}, with maximum compression strength of 0.63

MPa and thermal conductivity of 0.054 W m^{-1} K^{-1}. On the other hand, optimum density value

for APD-BTESB derived aerogels was determined as 0.70 g cm^{-3}, with higher maximum

compression strength ranging of 2.4 MPa and thermal conductivity of 0.079 W m^{-1} K^{-1}.
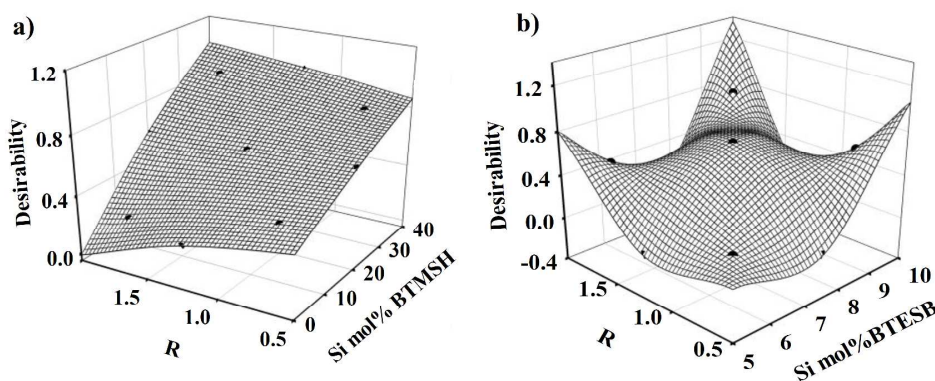
Figure 8. a) Desirability versus Si mol% of BTMSH and R for BTMSH derived aerogel-like monoliths, b) Desirability versus Si mol% of BTESB and R for BTESB derived aerogel-like monoliths.

Table 6. Optimal design points for BTMSH and BTESB derived aerogel-like monoliths with their predicted response values.

Bis-silane mol%	R	Density (g cm^{-3})	Thermal conductivity (W m^{-1} K^{-1})	Max. stress at break (MPa)	Desirability
BTMSH: 40 mol%	1.56	0.269	0.054	0.631	0.976
BTESB: 9.27 mol%	1.8	0.760	0.079	2.380	0.80

After the determination of APD-aerogel-like samples with optimized properties, our next attempt was to compare their important properties with the scCO$_2$ dried aerogel counterparts under the same preparation conditions. For both experimental approaches, we selected the design points that are near in terms of the preparation conditions to the defined optimized APD-aerogel-like monoliths, according to the formulations indicated in Table 6. The selected optimized samples have been synthesized by subjecting the wet gels to extra post-gelation washing with hexane so that all methanol and residual water could be removed. Then, several important properties, including physical and mechanical properties, of both types of samples

were compared with those from their scCO$_2$ dried counterparts - Table 7. It is interesting to

note that, by increasing the number of the post-gelation treatment cycles of monoliths with

hexane, the material properties of the sample have been improved over their previous values

at Table 4.

Table 7. Comparison of important physical and mechanical properties of optimized APD-

aerogel-like monoliths and scCO$_2$ dried aerogels under the same synthesis conditions.

Sample	Density (g cm^{-3})	Shrinkage (Diam.%)	BET (m^2 g^{-1})	Pore volume (cm^3 g^{-1})	Average pore diameter (nm)	Thermal conductivity (W m^{-1} K^{-1})	Max. stress at break (MPa)
SCD-B_40_R_1.25	0.22	11	82.2	3.5	170	0.060	0.523
APD-B_40_R_1.25	0.24	14	53.1	3.47	261	0.055	0.786
SCD-Bz_9_R_1.8	0.29	12	208.9	3.94	75	0.052	1.146
APD-Bz_9_R_1.8	0.52	26	155.1	1.81	47.4	0.075	2.658

As indicated, BTMSH derived aerogel-like samples are stronger than their SCD

counterparts with only marginal differences between density and thermal conductivity of both

samples. Sample photos shown in Figure 9a reveal that there are no major structural or

physical differences in both aerogel and aerogel-like samples derived from BTMSH, and,

both are strong and have enough structural integrity. However, compared to the SCD

aerogels, aerogel-like samples, due to the relatively higher shrinkage upon drying from

hexane, have exhibited less spring back or recovery of the gel initial size after drying. The

higher shrinkage caused to some extent the losing of porosity and surface area in the APD

aerogels. Analyzing the stress strain curves (Figure 9c), they revealed that the scCO$_2$ dried

BTMSH aerogel possesses slightly high elastic properties, confirmed by its higher strain

values, up to approximately 45% of the strain, when compared to the APD-aerogel-like

monoliths that compressed up to 36% of the strain.

In terms of BTESB derived samples, a 50% increase in the density along with significant

increase in the mechanical strength is shown for the aerogel-like samples when compared to

their scCO$_2$ dried counterparts. As mentioned before, BTESB derived APD-aerogel-like

monoliths have suffered higher dimensional shrinkage when compared to the BTMSH

derived samples. Therefore, a significant increase in density is noticed for the BTESB

aerogel-like samples (Figure 9b). It worth noting that, despite of higher *R* values for the

optimized BTESB samples, their surface area is still high. This confirms their relatively high

pore volume and extent of porosity even after large shrinkage with drying – Table 7.
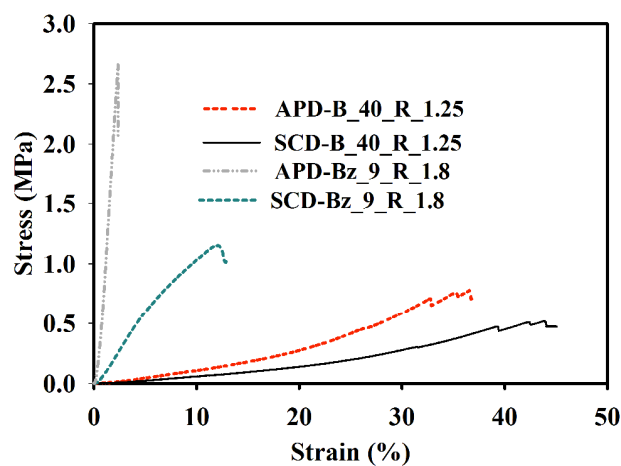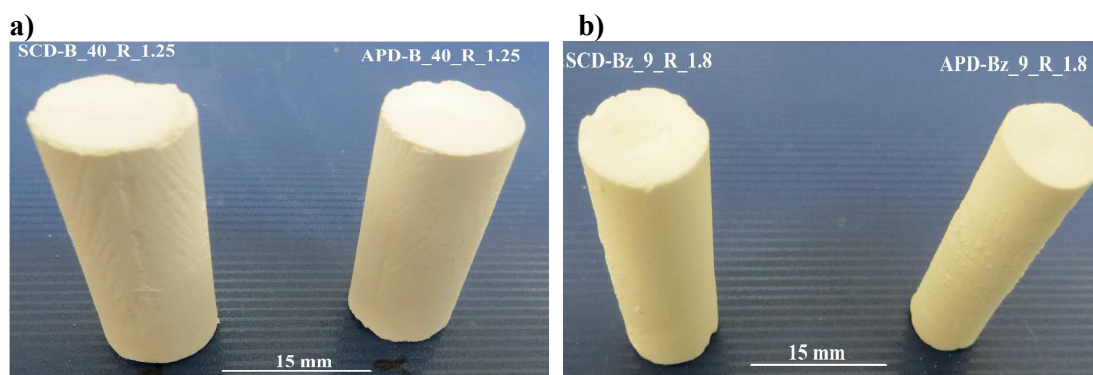
Figure 9. a) Optimized APD-BTMSH derived aerogel-like samples and their scCO$_2$ dried

counterparts and, b) optimized APD-BTESB derived aerogel-like samples versus their scCO$_2$

dried counterparts, c) stress-strain curves for monoliths in a) and b).

Scanning electron microscopy micrographs of both optimized APD samples and their

scCO$_2$ dried aerogel counterparts are shown in Figure 10, under the same preparation

conditions. The SEM micrographs of both types of samples revealed conformal polymer

coating on the silica that forms the skeletal framework of the aerogel. The optimized APD

crosslinked BTMSH derived aerogels retain a microstructure, which is to some extent

identical to that of aerogels dried under supercritical conditions. On the other hand, the

optimized crosslinked APD-BTESB derived aerogel monolith shows clear signs of collapse

(*i.e.* a virtual disappearance of mesoporosity and irregularities in the silica particles

morphology). This result is in agreement with the high extent of shrinkage and relatively low

surface area and porosity when compared to the scCO$_2$ dried aerogel, already discussed

before.

Overall, these results suggest that the properties of crosslinked aerogels dried from hexane

under ambient pressure are not very different from the properties of those dried

supercritically.

scCO₂ dried aerogels (a,c) **APD-aerogel-like samples (b,d)**

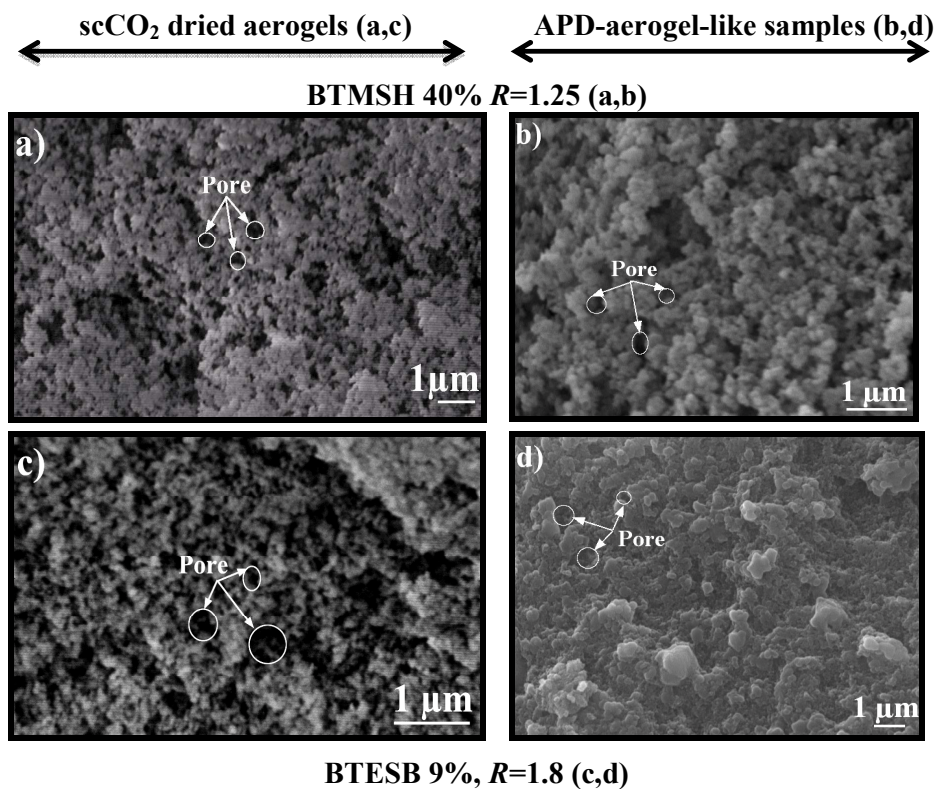**BTMSH 40% *R*=1.25 (a,b)**

BTESB 9%, *R*=1.8 (c,d)
Figure 10. SEM images of optimized APD and scCO₂ dried aerogels.

3.4 Evaluation of sample properties for Space applications

The properties of aerogel and aerogel-like materials should fulfill the requirements for service in the environments to which they will be exposed. The aerogels in this study are being developed for Space applications; therefore, the material properties should comply with the thermal characteristics of the Space environment. There are several standard tests to evaluate the material specification with the purpose of Space use [50]. These standards apply to materials used for structural, semi-structural, electronic, electrical as well as both manned and unmanned Space craft applications. The standards should consider some constrains that are specific to Space, *i.e.* vacuum and radiation. These constrains are applied in order to ensure that the material satisfies the requirements during mission. Vacuum outgassing [51] and thermal cycling [52] are two important examples of those important standard tests to qualify materials for Space use.

Vacuum outgassing test is applied to evaluate outgassing characteristics of the proposed

materials under high vacuum, when they are developed for use in the fabrication of spacecraft

and their associated equipment. The summary of results for the samples subjected to

outgassing is presented in Table 8, revealing that, for optimized APD-aerogel-like samples

and their scCO$_2$ dried aerogels, the RML values are far less than 1%, which indicates the

compatibility of samples with simulated thermal and vacuum characteristics of the Space

environment. The chemical structure inspection by ATR FT-IR also confirms that there are no

structural degradation/dissociation of the chemical bonds of the aerogels after 24 hours of

outgassing at $T = 125^oC$ – Figure SI_3a, b.

The thermogravimetric analysis indicated that both BTMSH and BTESB derived aerogels

are almost thermally stable, since there is no significant mass loss until $T = 125^oC$, except for

the mass loss of water adsorbed on the aerogel network - Figure SI_4.

Table 8. Vacuum outgassing data for optimized APD-aerogel-like samples and scCO$_2$ dried

aerogel samples.

Sample	TML %	RML %	WVR %
SCD-B_40_R_1.25	0.920±0.080	0.290±0.002	0.640±0.002
APD-B_40_ R_1.25	1.280±0.070	0.460±0.070	0.820±0.001
SCD-Bz_9_R_1.8	1.080±0.002	0.230±0.003	0.850±0.010
APD-Bz_9_R_1.8	1.500±0.001	0.460±0.002	1.040±0.007

Thermal cycling is the other standard test, in which material is subjected to a certain

number of thermal cycles under vacuum. The purpose of this test is to evaluate the capability

of the material to withstand thermal stresses in the intended Space environment. For this,

temperature oscillates within a defined temperature range in order to anticipate or evaluate the

material resistance to some deleterious, namely outgassing, fracture or cracking due to sudden

dimensional changes and so forth. Here in, the optimized APD and scCO$_2$ dried aerogel

samples were subjected to three successive thermal cycles by applying temperature in the

range of -78 to 125°C in each cycle, under vacuum. Subsequently, the tested samples were

inspected by visual examination, outgassing recording. Summary of the outgassing behavior

of the samples during three referred cycles is shown in Table 9. These results reveal that

samples are stable even after three thermal cycles.

Table 9. Thermal cycling data for optimized APD and scCO$_2$ dried aerogels.

Sample	1st thermal cycle		
	TML$_1$ (%)	RML$_1$ (%)	WVR$_1$ (%)
SCF-B_40_R_1.25	1.090 ± 0.006	0.580 + 0.003	0.510 ± 0.004
APD_B_40_R_1.25	0.960 ± 0.005	0.620 ± 0.003	0.340 ± 0.002
SCF-Bz_9_R_1.8	1.130± 0.006	0.560 ± 0.002	0.580 ± 0.004
APD-Bz_9_R_1.8	0.910 ± 0.002	0.780 ± 0.002	0.130 ± 0.001
	2nd thermal cycle		
	TML$_2$ (%)	RML$_2$ (%)	WVR$_2$ (%)
SCF-B_40_R_1.25	0.860 ± 0.130	0.290 ± 0.010	0.530 + 0.020
APD_B_40_ R_1.25	0.880 ± 0.130	0.200 ± 0.050	0.660 ± 0.050
SCF-Bz_9_R_1.8	1.030 ± 0.30	0.470 ± 0.030	0.560 ± 0.120
APD-Bz_9_R_1.8	1.000 ± 0.13	0.410 ± 0.030	0.590 ± 0.200
	3rd thermal cycle		
	TML$_3$ (%)	RML$_3$ (%)	WVR$_3$ (%)
SCF-B_40_R_1.25	1.430 ± 0.270	0.030 ± 0.007	1.400 ± 0.007
APD_B_40_ R_1.25	0.950 ± 0.050	0.310 ± 0.041	0.640 ± 0.035
SCF-Bz_9_R_1.8	0.840 ± 0.100	0.040 ± 0.040	0.800 ± 0.140
APD-Bz_9_R_1.8	1.270 ± 0.200	0.540 ± 0.010	0.730 ± 0.210

4. Conclusion

In summary, ambient pressure dried silica aerogels with different underlying silica

structures have been synthesized. The polymer crosslinked silica aerogel monoliths developed

here can be dried under ambient pressure from hexane with no need for risky supercritical

fluid extraction. Herein, the key properties of APD-aerogel-like materials, including bulk

density, thermal conductivity and mechanical properties, were studied and modeled by using a

statistical design of experiments. The empirical models derived for each type of aerogel-like samples allowed us to define the optimized preparation conditions by means of a desirability function that included all the referred key properties. Comparing the optimized APD aerogels' properties with those of their scCO$_2$ dried counterparts, we proved the similarity in the some properties with ~2× increase in the mechanical strength, which confirmed the adequacy of the proposed synthesis and drying method. Also, the crosslinked aerogels of this study are more than 400× stronger than the underlying plain silica framework, and thus they have been able to withstand the surface tension forces during ambient pressure drying. Such drastic increase in mechanical strength was accompanied by less than two time increase in the bulk density for BTMSH based aerogel-like samples over their nonreinforced counterparts. Additionally, the optimized aerogel-like and aerogel samples of this study have been inspected in terms of their material characteristics for use at intended Space applications. It has been shown that the material characteristics of the developed aerogels are suitable for the simulated Space environment condition. This appears to be the first report on aerogels addressing successfully the aerogels' material specification for Space environments.

Finally, monolithic materials developed here have a broad practical impact. In fact, due to their hydrophobicity, higher mechanical strength and the need of simple ambient pressure drying, they can replace their supercritical counterparts in some applications, enabling large-scale production.

Supporting Information Available: Additional figures and tables are supplied as

supplementary information. This material is available free of charge via the Internet at

http://pubs.acs.org.

5. References

1.   Dorcheh, A. S.; Abbasi, M. H. Silica Aerogel; Synthesis, Properties and

Characterization. *J. Mater. Proc. Technol.* **2008,** *199* 10-26.

2.   Maynard, R. Elastic and Thermal-Properties of Hierarchical Structures - Application

to Silica Aerogels. *Physica A* **1989,** *157*, 601−609.

3.   Fricke, J. Aerogels and Their Applications. *J. Non-Cryst. Solids* **1992,** *147*, 356−362.

4.   Bernasconi, A.; Sleator, T.; Posselt, D.; Ott, H. R. Dynamic Technique for

Measurement of the Thermal-Conductivity and the Specific-Heat - Application to Silica

Aerogels. *Rev. Sci. Instrum.* **1990,** *61*, 2420−2426.

5.   Jones, S. M. Aerogel: Space Exploration Applications. *J. Sol-Gel Sci. Technol.* **2006,**
40, 351–357.

6.   Leventis, N.; Palcezer, A.; Mccorkle, L. Nanoengineered Silica-Polymer Composite

Aerogels with No Need for Supercritical Fluid Drying. *J. Sol-Gel Sci.Tech.* **2005,** *35*, 99–105.

7.   Wei, T.-Y.; Lu, S.-Y.; Chang, Y.-C. Transparent, Hydrophobic Composite Aerogels

with High Mechanical Strength and Low High-Temperature Thermal Conductivities. *J. Phys.*

Chem. B **2008,** *112* (38), 11881–11886.

8.   Wu, G.; Yu, Y.; Chenga, X.; Zhang, Y. Preparation and Surface Modification

Mechanism of Silica Aerogels via Ambient Pressure Drying. *Mater. Chem. Phys.* **2011,** *129*

(1–2), 308–314.

9.   Yang, H.; Kong, X.; Zhang, Y.; Wu, C.; Cao, E. Mechanical Properties of Polymer-

Modified Silica Aerogels Dried under Ambient Pressure. *J. Non-Cryst. Solids* **2011,** *357*,

3447–3453.

10.   Durães, L.; Ochoa, M.; Rocha, N.; Patrício, R.; Duarte, N.; Redondo, V.; Portugal, A.

Effect of the Drying Conditions on the Microstructure of Silica Based Xerogels and Aerogels.

J. Nanosci. Nanothnol. **2012,** *12*, 6828-34.

11.   Hwang, S.-W.; Jung, H.-H.; Hyun, S.-H.; Ahn, Y.-S. Effective Preparation of Crack-

Free Silica Aerogels via Ambient Drying. *J. Sol-Gel Sci. Techn.* **2007,** *41*, 139-146.

12.   Kim, C. E.; Yoon, J. S.; Hwang, H. J. Synthesis of Nanoporous Silica Aerogel by

Ambient Pressure Drying. *J. Sol-Gel Sci. Techn.* **2009,** *49*, 47-52.

13.   Bhagat, S. D.; Kim, Y.-H.; Moon, M.-J.; Ahn, Y.-S.; Yeo, J.-G. A Cost-Effective and

Fast Synthesis of Nanoporous SiO_2 Aerogel Powders Using Water-Glass via Ambient

Pressure Drying Route. *Solid State Sci.* **2007,** *9*, 628-635.

14.   Smith, D. M.; Deshpande, R.; Brinker, C. J. Preparation of Low-Density Aerogels at

Ambient Pressure. *Mat. Res. Soc. Symp. Proc.* **1992,** *271*, 567–572.

15.   Prakash, S. S.; Brinker, C. J.; Hurd, A. J.; Rao, S. M. Silica Aerogel Films Prepared at

Ambient Pressure by Using Surface Derivatization to Induce Reversible Drying Shrinkage.

Nature **1995,** *374*, 439–443.

16.   Rao, A. P.; Rao, A. V.; Pajonk, G. M. Hydrophobic and Physical Properties of the

Ambient Pressure Dried Silica Aerogels with Sodium Silicate Precursor Using Various

Surface Modification Agents. *Appl. Surf. Sci.* **2007,** *253*, 6032–6040.

17.   Rao, A. P.; Rao, A. V.; Gurav, J. L. Effect of Protic Solvents on the Physical

Properties of the Ambient Pressure Dried Hydrophobic Silica Aerogels Using Sodium Silicate

Precursor. *J. Porous Mater.* **2008,** *15*, 507–512.

18.   Kartal, A. M.; Erkey, C. Surface Modification of Silica Aerogels by

Hexamethyldisilazane–Carbon Dioxide Mixtures and Their Phase Behavior. *J. Supercrits.

Fluids* **2010,** *53*, 115–120.

19.   Hegde, N. D.; Rao, A. V. Physical Properties of Methyltrimethoxysilane Based Elastic

Silica Aerogels Prepared by the Two-Stage Sol–Gel Process. *J. Mater. Sci. Lett.* **2007,** *42*

6965-6971.

20.   Nadargi, D. Y.; Latthe, S. S.; Hirashima, H.; Rao, A. V. Studies on Rheological

Properties of Methyltriethoxysilane (MTES) Based Fexible Superhydrophobic Silica

Aerogels. *Micropor. Mesopor. Mater.* **2009,** *117*, 617-626.

21.   Martin, L.; Osso, J. O.; Ricart, S.; Roig, A.; Garci, O.; Sastre, R. Organo-Modified

Silica Aerogels and Implications for Material Hydrophobicity and Mechanical Properties. *J.

Mater. Chem.* **2008,** *18*, 207–213.

22.   Maleki, H.; Duraes, L.; Portugal, A. An Overview on Silica Aerogels Synthesis and

Different Mechanical Reinforcing Strategies. *J. Non-Cryst. Solids* **2014,** *385,* 55-74.

23.   Leventis, N. Three-Dimensional Core-Shell Superstructures: Mechanically Strong

Aerogels. *Acc. Chem. Res.* **2007** *40*, 874–884.

24.   Adachi, T.; Sakka, S. Effect of Formamide Additive on the Chemistry of Silica Sol-

Gels: Part I: NMR of Silica Hydrolysis. *J. Non-Cryst. Solids* **1986,** *79*, 177-194.

25.   Kirkbir, F.; Murata, H.; Meyers, D.; Chaudhuri, S. R.; Sarkar, A. Drying and Sintering

of Sol-Gel Derived Large SiO_2 Monoliths. *J. Sol-Gel Sci. Technol.* **1996,** *6*, 203-217.

26.   Durães, L.; Maia, A.; Portugal, A. Effect of Additives on the Properties of Silica

Based Aerogels Synthesized from Methyltrimethoxysilane (MTMS). *In: Proceedings of*

International Seminar on Aerogels,International Society for Advancement of Supercritial

Fluids (ISASF) and Hamburg University of Technology (TUHH), Hamburg **2014**, 33-43.

27.   Dullien, F. a. L. *Porous Media: Fluid Transport and Pore Structure*; Academic Press:

San Diego, 1992.

28.   Randall, J. P.; Meador, M. a. B.; Jana, S. C. Tailoring Mechanical Properties of

Aerogels for Aerospace Applications. *ACS Appl. Mater. Interfaces* **2011,** *3*, 613-626.

29.   Maleki, H.; Duraes, L.; Portugal, A. Synthesis of Lightweight Polymer-Reinforced

Silica Aerogels with Improved Mechanical and Thermal Insulation Properties for Space

Applications. *Micropor. Mesopor. Mater.* **2014,** *197*, 116–129.

30.   Montgomery, D. C. *Design and Analysis of Experiments* [Online]; 6th ed. ed; John
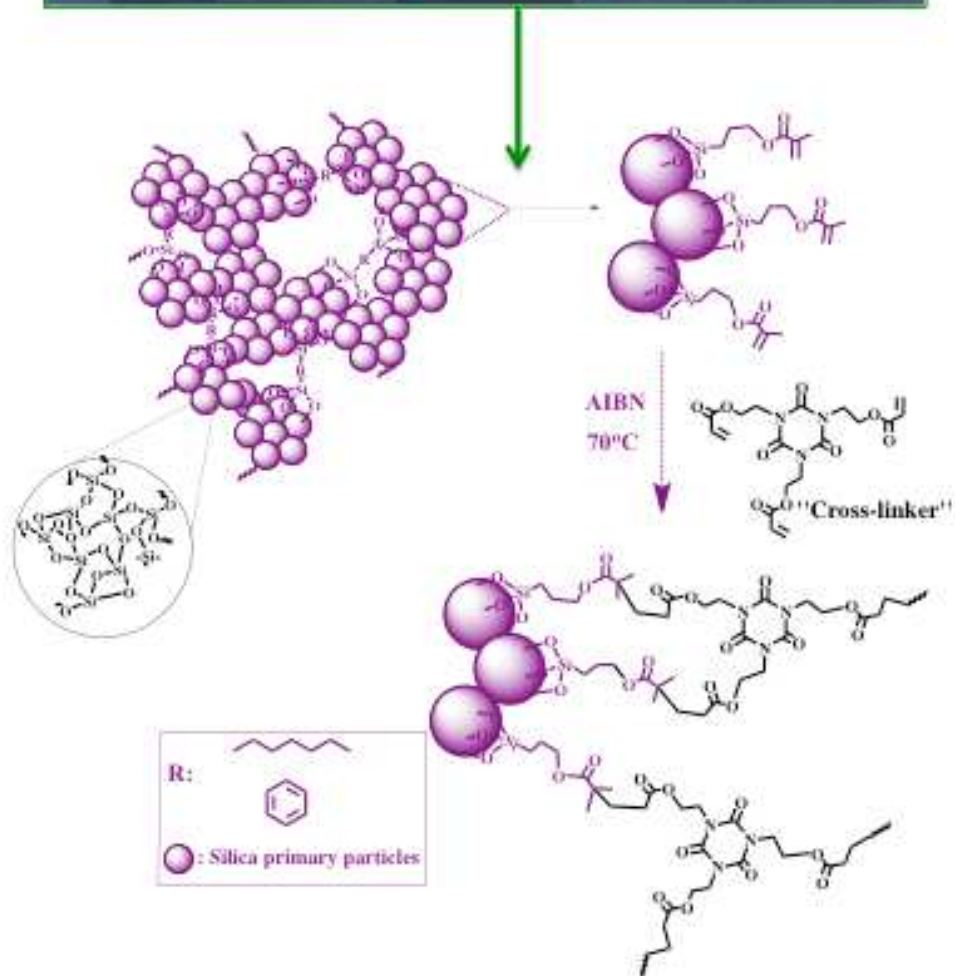
Wiley & Sons New York, USA, 2006.

31.   Goupy, J.; Creighton, L. *Introduction to Design of Experiments with JMP Examples* [Online]; third ed; SAS Institute Inc. : Cary, NC, USA, 2007.

32.   White, L. S.; Bertino, M. F.; Kitchen, G.; Young, J.; Newton, C.; Al-Soubaihi, R.; Saeed, S.; Saoud, K. Shortened Aerogel Fabrication Times using an Ethanol-Water Azeotrope as a Gelation and Drying Solvent. *J. Mater. Chem. A* **2015,** *3*, 762-772.

33.   Mulik, S.; Sotiriou-Leventis, C.; Churu, G.; Lu, H.; Leventis, N. Cross-Linking 3D Assemblies of Nanoparticles into Mechanically Strong Aerogels by Surface-Initiated Free-Radical Polymerization. *Chem. Mater.* **2008,** *20*, 5035–5046.

34.   Maleki, H.; Durães, L.; Portugal, A. Synthesis of Mechanically Reinforced Silica Aerogels via Surface-Initiated Reversible Addition-Fragmentation Chain Transfer (RAFT) Polymerization. *J. Mater. Chem. A* **2015,** *3*, 1594-1600.

35.   Chidambareswarapattar, C.; Mccarver, P. M.; Luo, H.; Lu, H.; Sotiriou-Leventis, C.; Leventis, N. Fractal Multiscale Nanoporous Polyurethanes: Flexible to Extremely Rigid Aerogels from Multifunctional Small Molecules. *Chem. Mater.* **2013,** *25* 3205–3224.

36.   Mohite, D. P.; Larimore, Z. J.; Lu, H.; Mang, J. T.; Sotiriou-Leventis, C.; Leventis, N. Monolithic Hierarchical Fractal Assemblies of Silica Nanoparticles Cross-Linked with Polynorbornene via ROMP: A Structure−Property Correlation from Molecular to Bulk through Nano. *Chem. Mater.* **2012,** *24*, 3434−3448.

37.   Nguyen, B. N.; Meador, M. a. B.; Tousley, M. E.; Shonkwiler, B.; Mccorkle, L.; Scheiman, D. A.; Palczer, A. Tailoring Elastic Properties of Silica Aerogels Cross-linked with Polystyrene. *ACS Appl. Mater. Interfaces* **2009,** *1* 621-630.

38.   Feng, L.; Zhang, Y.; Xi, J.; Zhu, Y.; Wang, N.; Xia, F.; Jiang, L. Petal Effect: A

Superhydrophobic State with High Adhesive Force. *Langmuir* **2008,** *24*, 4114−4119.

39.   Leventis, N.; Chidambareswarapattar, C.; Bang, A.; Sotiriou-Leventis, C. Cocoon-in-

Web-Like Superhydrophobic Aerogels from Hydrophilic Polyurea and Use in Environmental

Remediation. *ACS Appl. Mater. Interfaces* **2014,** (6), 6872−6882.

40.   Wang, X.; Jana, S. C. Tailoring of Morphology and Surface Properties of Syndiotactic

Polystyrene Aerogels. *Langmuir* **2013,** *29*, 5589-98.

41.   Ilhan, U. F.; Fabrizio, E. F.; Mccorkle, L.; Scheiman, D. A.; Dass, A.; Palczer, A.;

Meador, M. a. B.; Johnston, J. C.; Leventis, N. Hydrophobic Monolithic Aerogels by

Nanocasting Polystyrene on Amine-Modified Silica. *J. Mater. Chem.* **2006,** *16* 3046-3054.

42.   Lee, J. K.; Gould, G. L.; Rhine, W. Polyurea Based Aerogel for a High Performance

Thermal Insulation Material. *J. Sol-Gel Sci.Technol.* **2009,** *49*, 209–220.

43.   Meador, M. a. B.; Vivod, S. L.; Mccorkle, L.; Quade, D.; Sullivan, R. M.; L.N.

Ghson, C.; Capaclona, L. A. Reinforcing Polymer Cross-linked Aerogels with Carbon

Nanofibers. *J. Mater. Chem.* **2008,** *18*, 1843-1852.

44.   Meador, M. a. B.; Weber, A. S.; Hindi, A.; Naumenko, M.; Mccorkle, L.; Quade, D.;

Vivod, S. L.; Gould, G. L.; White, S.; Deshpande, K. Structure-Property Relationships in

Porous 3D Nanostructures: Epoxy-Cross-linked Silica Aerogels Produced using Ethanol as

the Solvent. *ACS Appl. Mater. Interfaces* **2009,** *1*, 894-906.
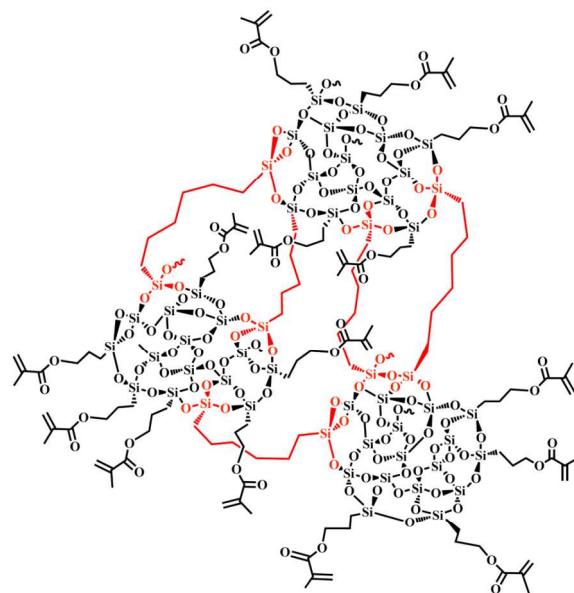
45.   Capadona, L. A.; Meador, M. a. B.; Alunni, A.; Fabrizio, E. F.; Vassilaras, P.; Leventis, N. Flexible, Low-density Polymer Crosslinked Silica Aerogels. *Polymer* **2006,** *47*, 5754-5761.

46.   Meador, M. a. B.; Nguyen, B. N.; Quade, D.; Vivod, S. L. Epoxy Reinforced Aerogels Made Using a Streamlined Process. *ACS Appl. Mater. Interfaces* **2010,** *2*, 2162-2168.

47.   Meador, M. a. B.; Fabrizzio, E. F.; F. Ilhan, A. D.; Zhang, G.; Vassilaras, P.; Johnston, J. C.; Leventis, N. Crosslinking Amine Modified Silica Aerogels with Epoxies: Mechanically Srong Lightweight Porous Materials. *Chem. Mater.* **2005,** *17*, 1085-1098.

48.   Derringer, G.; Suich, R. Simultaneous Optimization of Several Response Variables. *J. Qual. Technol.* **1980,** *12*, 214-219.

49.   Cojocaru, C.; Khayet, M.; Zakrzewska-Trznadel, G.; Jaworska, A. Modeling and Multi-Response Optimization of Pervaporation of Organic Aqueous Solutions Using Desirability Function Approach. *J. Hazard. Mater.* **2009,** *167* 52–63.

50.   Data for Selection of Space Materials and Processes. *European Cooperation for Space Standardization, ECSS-Q-70-71A rev. 1* **2004**.

51.   Thermal Vacuum Outgassing Test for the Screening of Space Materials. *European Cooperation for Space Standardization, ECSS-Q-ST-70-02C* **2008**.

52.   Thermal Testing for the Evaluation of Space Materials, Processes, Mechanical parts and Assemblies. *European Cooperation for Space Standardization, ECSS-Q-ST-70-04C* **2008**.
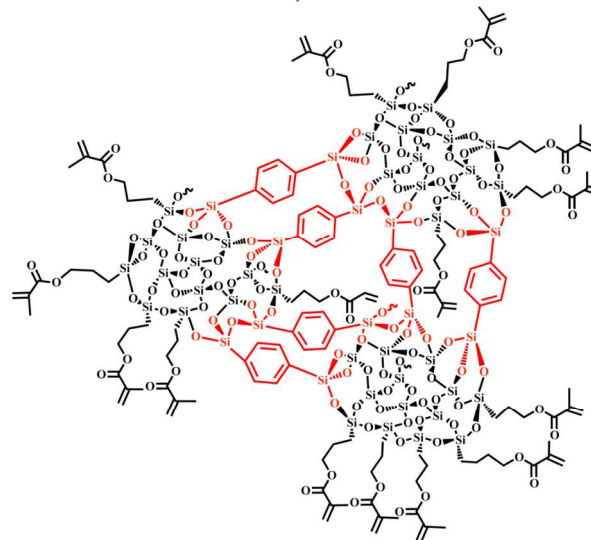
1
2
3
4
5
6
7
8
9
10
11
12
13
14
15
16
17
18
19
20
21
22
23
24
25
26
27
28
29
30
31
32
33
34
35
36
37
38
39
40
41
42
43
44
45
46
47
48
49
50
51
52
53
54
55
56
57
58
59
60

TOC:

Macroscopic view of aerogels:

APD-B_40_R_1.25   APD-Bz_9_R_1.8

15 mm

AIBN
70°C

"Cross-linker"

R:

: Silica primary particles

Microscopic view of aerogels

a)

b)

315x630mm (96 x 96 DPI)

136x115mm (300 x 300 DPI)

TMOS + Bridged bis-silane co-precursors + TMSPM

Sol-gel

AIBN

70°C

"Cross-linker"

R:

◯ **: Silica primary particles**
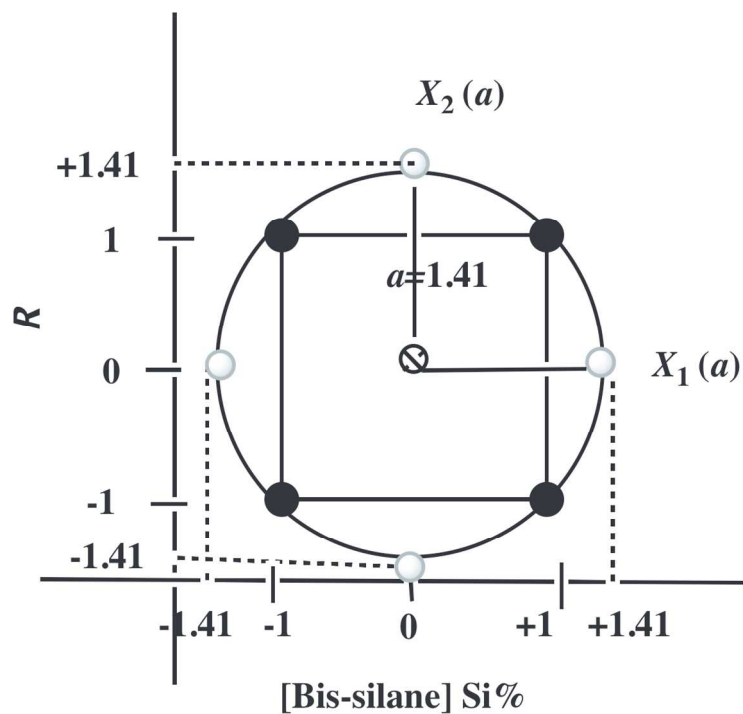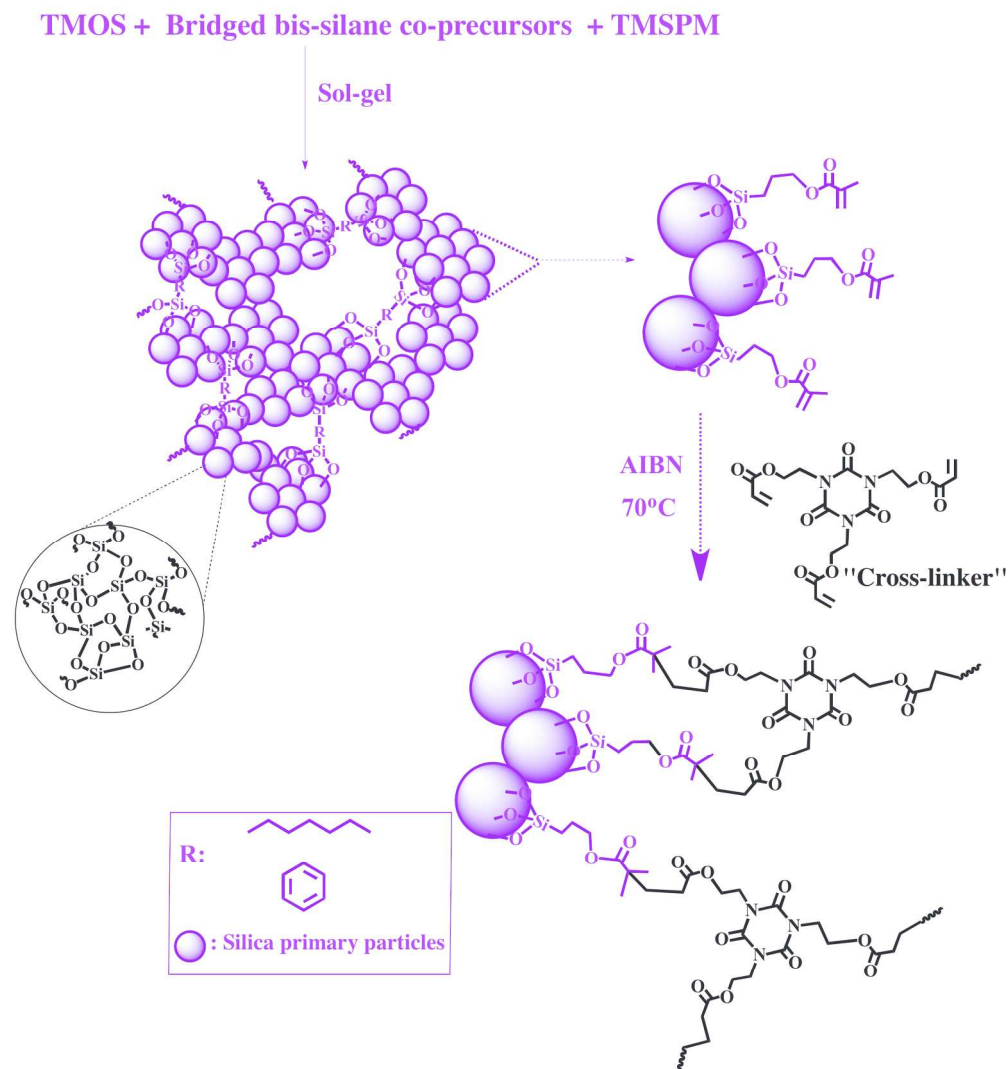
192x205mm (300 x 300 DPI)

191x119mm (300 x 300 DPI)

$\theta = 151° \pm 15°$

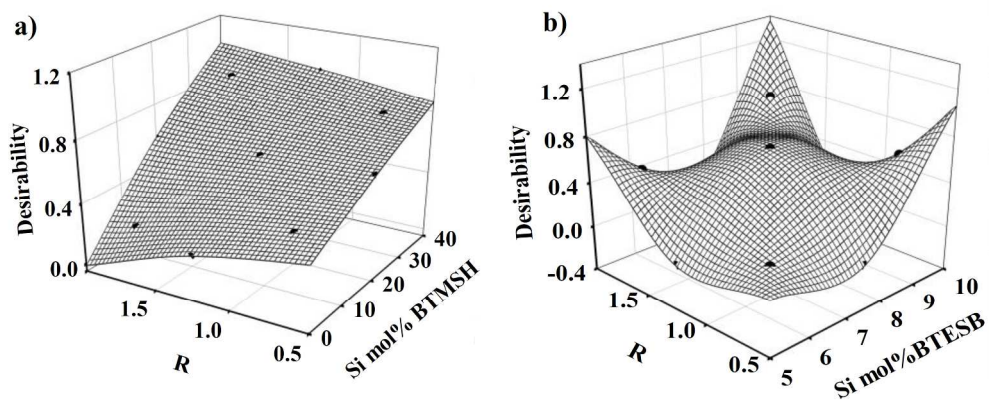**a)** B_40_R_1.25

$\theta = 102° \pm 4°$

b) Bz_9_R_1.8

$\theta = 100° \pm 5°$

c) B_0_R_1.25
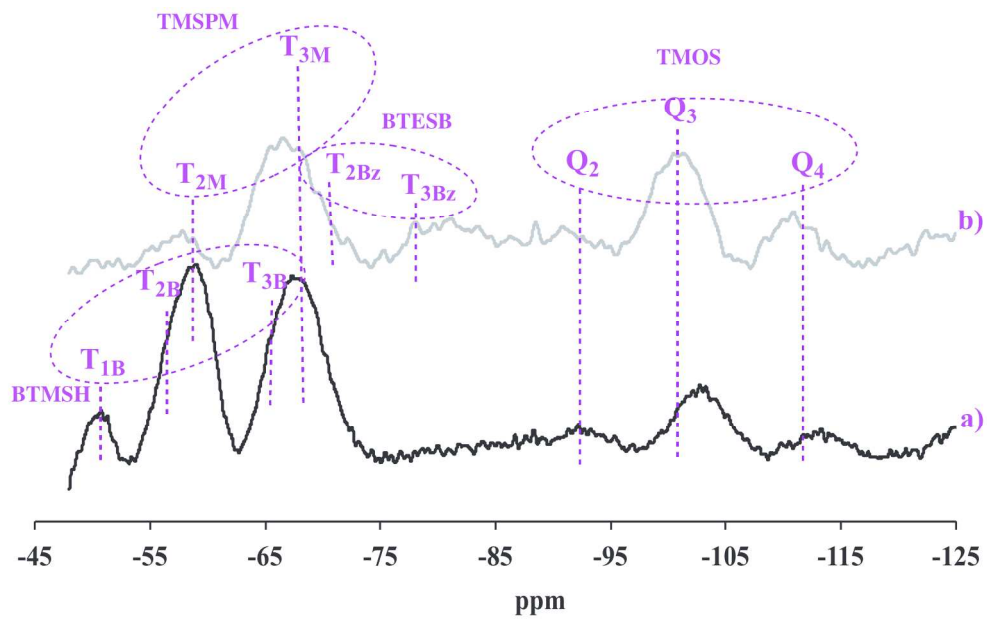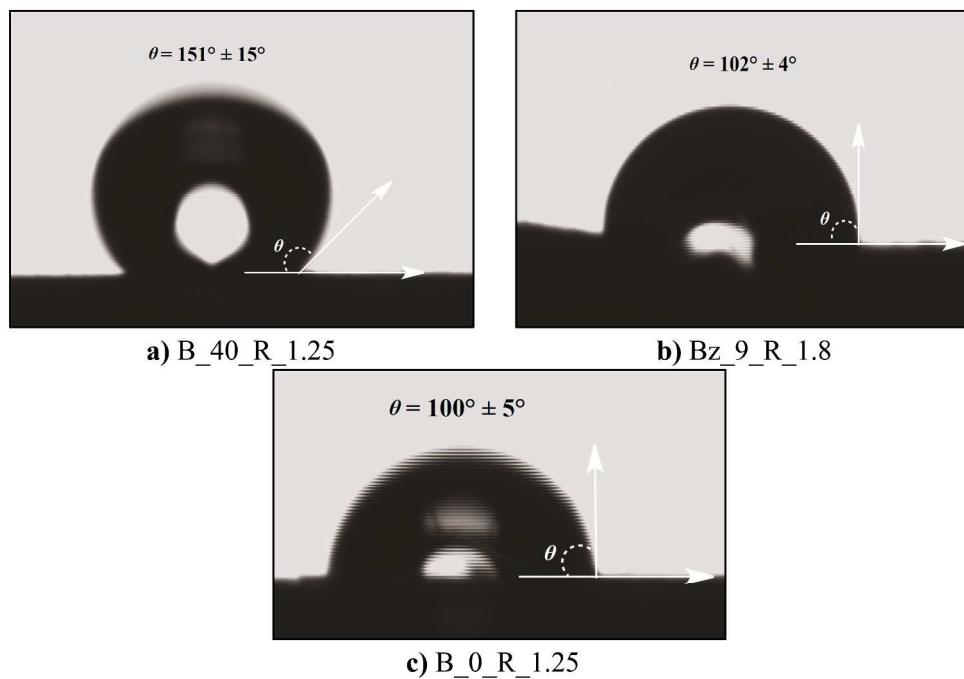
1367x931mm (96 x 96 DPI)

1613x1051mm (96 x 96 DPI)

1
2
3
4
5
6
7
8
9
10
11
12
13
14
15
16
17
18
19
20
21
22
23
24
25
26
27
28
29
30
31
32
33
34
35
36
37
38
39
40
41
42
43
44
45
46
47
48
49
50
51
52
53
54
55
56
57
58
59
60
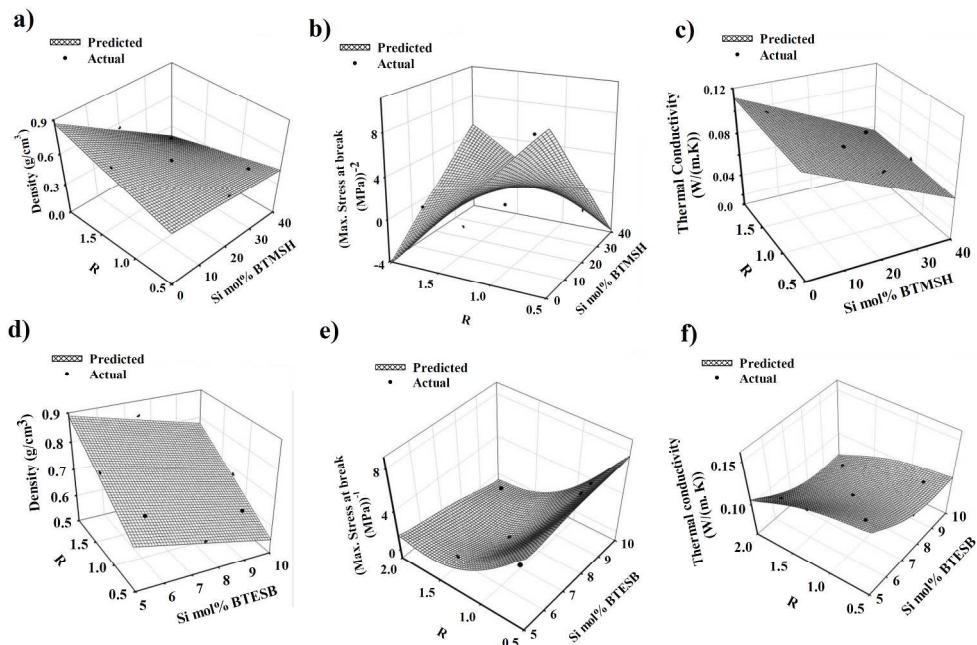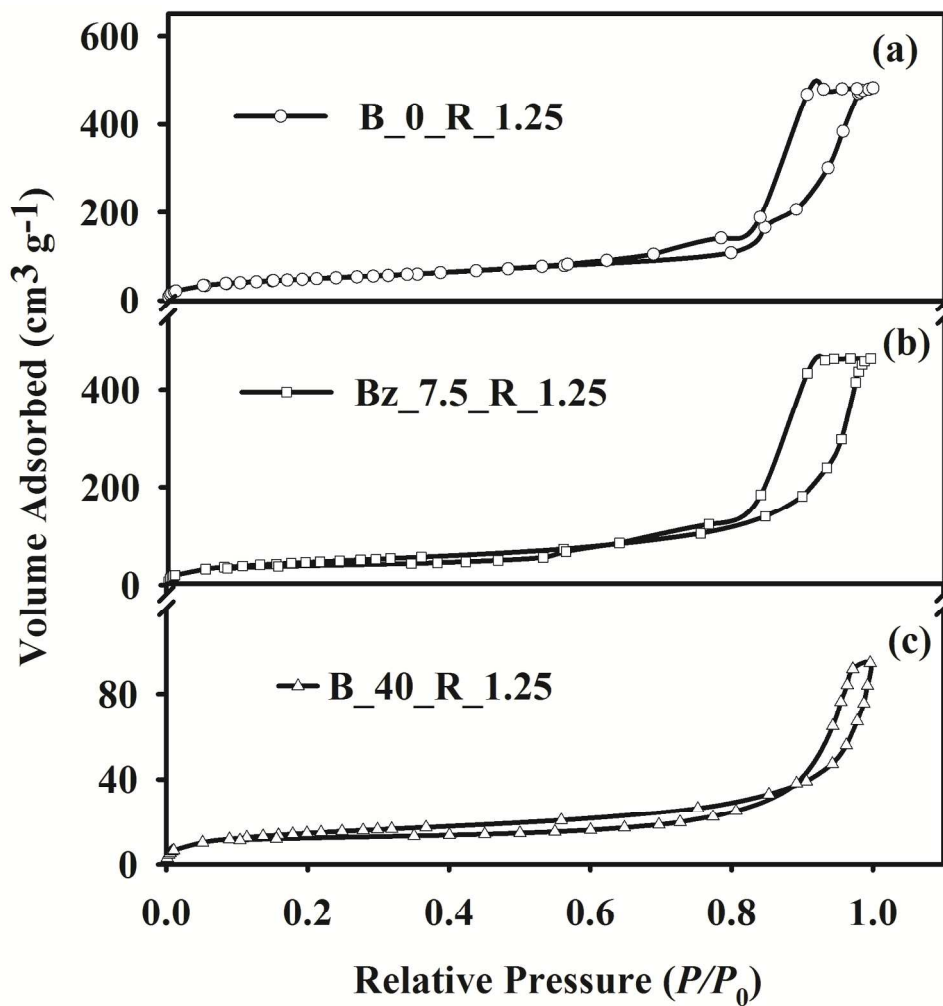
353x355mm (150 x 150 DPI)

1230x499mm (96 x 96 DPI)

1494x1172mm (96 x 96 DPI)

scCO₂ dried aerogels (a,c)   APD-aerogel-like samples (b,d)

BTMSH 40% *R*=1.25 (a,b)

BTESB 9%, *R*=1.8 (c,d)

1236x1031mm (96 x 96 DPI)